

Volatility Modeling with Rough Paths: A Signature-Based Alternative to Classical Expansions

Elisa Alòs^{*}, Òscar Burés^{†§}, Rafael de Santiago[§] and Josep Vives^{†‡}

August 4, 2025

Abstract

We compare two methodologies for calibrating implied volatility surfaces: a second-order asymptotic expansion method derived via Malliavin calculus, and a data-driven approach based on path signatures from rough path theory. The former, developed in Alòs et al. (2015), yields efficient and accurate calibration formulas under the assumption that the asset price follows a Heston-type stochastic volatility model. The latter models volatility as a linear functional of the signature of a primary stochastic process, enabling a flexible approximation without requiring a specific parametric form.

Our numerical experiments show that the signature-based method achieves calibration accuracy comparable to the asymptotic approach when the true dynamics are Heston. We then test the model in a more general setting where the asset follows a rough Bergomi volatility process—a regime beyond the scope of the asymptotic expansion—and show that the signature approach continues to deliver accurate results. These findings highlight the model-independence, robustness and adaptability of signature-based calibration methods in settings where volatility exhibits rough or non-Markovian features.

Keywords: Stochastic volatility, fractional volatility, rough path theory, path signature, implied volatility calibration.

JEL Classification: G13, C63, C58.

MSC 2020: 60L70, 60H10, 91G20, 91G60, 60G22.

1 Introduction

The realization that constant-volatility models could not account for effects like clustering, heavy tails, and *smiles* prompted the extension of the Black–Scholes framework to include stochastic volatility. Early models addressed these limitations by introducing a second (correlated) Brownian motion to govern the volatility, yielding more realistic asset price dynamics. This line of research, initiated by Hull and White (1987), Wiggins (1987), Stein and Stein (1991), and Heston (1993), has given rise to a broad and influential literature in mathematical finance.

A particularly influential part of the literature has focused on developing closed-form approximation formulas for implied volatility through asymptotic expansions and perturbation methods applied to parametric models, such as Heston and SABR. These approximations aim to facilitate

^{*}Universitat Pompeu Fabra and Barcelona School of Economics, Department of Economics and Business. Ramón Trias Fargas 25-27, 08005, Barcelona, Spain.

[†]Departament de Matemàtica Econòmica, Financera i Actuarial. Diagonal 690–696, 08034 Barcelona, Spain.

[§]IESE Business School, Department of Managerial Decision Sciences. Av. Pearson 21, 08034 Barcelona, Spain.

[‡]Institut de Matemàtiques, Universitat de Barcelona. Gran Via de les Corts, 585, 08007 Barcelona, Spain.

Elisa Alòs, Rafael de Santiago and Josep Vives partially supported by grant PID2020-118339GB-I00 (2021–2025), Ministerio de Ciencia e Innovación. Òscar Burés supported by program AGAUR-FI ajuts (2025 FI-1 00580).

the calibration of model parameters to market-observed implied volatility surfaces. Efficient calibration is a central task in financial practice, as option prices are typically quoted via implied volatilities, and model parameters must be inferred by inversion. Contributions to this area include, among others, Hagan et al. (2002), Fouque et al. (2003), De Santiago et al. (2008), Antonelli and Scarlatti (2009), Benhamou et al. (2009, 2010a,b), Forde et al. (2010), Forde and Jacquier (2011), Forde et al. (2011), Alòs (2012), Medvedev and Scaillet (2007), Lorig et al. (2013) and Alòs et al. (2015).

While these parametric models and their expansions have proven theoretically elegant and computationally tractable, they also come with important limitations. Relying on a fixed model structure may restrict flexibility and hinder the model’s ability to capture certain stylized features observed in market data. In addition, the presence of multiple stochastic drivers often increases computational complexity, requiring the use of numerical tools such as Fourier transforms, Monte Carlo methods, or finite-difference PDE solvers. Moreover, a growing body of empirical evidence suggests that volatility exhibits rough, fractional-like behavior that traditional Markovian models struggle to reproduce. This has led to increased interest in fractional (rough) volatility models, such as those introduced in Comte and Renault (1998), Alòs et al. (2007), and Fukasawa (2017), which more accurately reflect the observed structure of the implied volatility surface and align with empirical evidence on the roughness of volatility paths (e.g., Bayer et al. (2016), Gatheral et al. (2018)).

In response to these challenges, a more recent line of research has embraced non-parametric, data-driven approaches that aim to learn volatility dynamics directly from observed paths, rather than specifying a rigid structural model. A prominent example of this paradigm is the use of rough path theory and signature methods, originally introduced in Chen (1957) and rigorously developed in Lyons (1998). The signature of a path (to be defined precisely below) consists of its iterated integrals and encodes its temporal features into a rich algebraic structure. Over the years, these ideas have found applications in machine learning, time series analysis, and mathematical finance (e.g., Bühler et al. (2020), Arribas et al. (2020), Cuchiero et al. (2023)). Because it relies on functional features rather than a parametric form, signature-based modeling is well suited for capturing behaviors observed in rough volatility models.

In this paper, we compare these two modeling approaches. On the one hand, we examine the parametric methodology of Alòs et al. (2015), which uses Malliavin calculus to derive a second-order expansion of implied volatility in the Heston model. This method, although model-specific, is remarkably precise and computationally efficient. On the other hand, we present a model-free approach based on signature-based learning, in which the volatility is approximated by a linear functional of the truncated signature of a primary noise process. Our goal is not only to compare their performance under a Heston regime, but also to assess how well the signature method generalizes when the underlying volatility deviates from the Heston structure.

To make the paper self-contained, in Section 2 we review the second-order expansion technique of Alòs et al. (2015), highlighting its mathematical structure and practical strengths. Section 3 introduces the core elements of rough path theory needed to define and compute path signatures, including p -variation, multiplicativity, and the extension theorem. In Section 4, we develop the signature-based stochastic volatility model, explain the algorithm for numerical implementation, and describe the training procedure. Section 5 presents the numerical results comparing both methods under various settings, including both uncorrelated and correlated Heston dynamics as in Alòs et al. (2015). We conclude with an additional example under rough Bergomi dynamics to highlight the method’s power and versatility.

2 A Second-Order Approximation to the Implied Volatility

The objective of this section is to provide a concise overview of the second-order approximation to the implied volatility derived in Alòs et al. (2015). For full proofs and theoretical justifications, we refer the reader to the original paper. Here we will only use the estimates obtained with this methodology as a reference. Specifically, we will compare the calibration results of our

signature-based model against those obtained using the parametric Heston framework, evaluating the accuracy of both approaches.

Assume that, for $t \in [0, T]$, the stock price follows the dynamics

$$dS_t = rS_t dt + \sigma_t S_t d(\rho W_t + \sqrt{1 - \rho^2} B_t) \quad (2.1)$$

under a risk neutral probability \mathbb{P} , where $r \geq 0$ is the constant instantaneous interest rate, W and B are independent standard Brownian motions defined in the complete probability space $(\Omega, \mathcal{F}, \mathbb{P})$, and $\rho \in (-1, 1)$. We also assume that the volatility process σ_t satisfies

$$d\sigma_t^2 = \kappa(\theta - \sigma_t^2)dt + \nu\sqrt{\sigma_t^2}dW_t, \quad (2.2)$$

with $2\kappa\theta \geq \nu^2$. We denote by $\mathcal{F}^W = \{\mathcal{F}_t^W; t \in [0, T]\}$ and $\mathcal{F}^B = \{\mathcal{F}_t^B; t \in [0, T]\}$ the filtrations generated, respectively, by W and B , and we define \mathcal{F} as the collection of sigma algebras $\mathcal{F}_t^W \vee \mathcal{F}_t^B$ for each $t \in [0, T]$, that is, $\mathcal{F} := \mathcal{F}^W \vee \mathcal{F}^B$. Equations (2.1) and (2.2) constitute what is known as the Heston model.

If we let $X_t := \ln S_t$, the price of a European call option at time t with strike K and maturity T is given by

$$V_t = e^{-r(T-t)} E_t[(e^{X_T} - K)^+],$$

where $E_t[\cdot] := E[\cdot | \mathcal{F}_t]$. For a constant volatility σ , and letting $k = \ln K$, the above general expression has the well-known analytical solution

$$V_t = \text{BS}(T, t, X_t, k, \sigma) = e^{X_t} \Phi(d_+) - e^{k-r(T-t)} \Phi(d_-),$$

where Φ is the cumulative distribution function of a standard Gaussian random variable, and

$$d_{\pm} = \frac{X_t - k + r(T-t)}{\sigma\sqrt{T-t}} \pm \frac{\sigma}{2}\sqrt{T-t}.$$

When volatility is not constant, the option price becomes

$$V_t = \text{BS}(T, t, X_t, k, v_t) := e^{X_t} \Phi(d_+) - e^{k-r(T-t)} \Phi(d_-),$$

where

$$d_{\pm} = \frac{X_t - k + r(T-t)}{v_t\sqrt{T-t}} \pm \frac{v_t}{2}\sqrt{T-t}$$

and

$$v_t = \sqrt{\frac{\int_t^T E_t(\sigma_s^2) ds}{T-t}}.$$

Let V_t^{mkt} be the market price at time t of a European call option with maturity T and strike K . As the BS function is invertible in the argument v_t , we can define the implied volatility as the unique $I(T, K)$ satisfying the equality

$$\text{BS}(T, t, X_t, k, I(T, K)) = V_t^{mkt}.$$

Since even in the simplest stochastic volatility models it is generally not feasible to derive closed-form expressions for the implied volatility surface, a variety of approximation methods have been developed to estimate $I(T, K)$.

The method in Alòs et al. (2015) proceeds in three steps. First, an approximation to the option price is derived. Based on this, a second-order closed-form expression for the implied volatility is obtained with the help of Malliavin calculus. Finally, using the term structure of at-the-money (ATM) options, the model parameters—including the mean-reversion rate—are calibrated. Starting from equations (2.1) and (2.2), the authors deduce the following approximations to the implied volatility.

When the option is close to maturity ($T \rightarrow 0$), the implied volatility can be written as:

$$I(0, K) \approx \sigma_0 - \frac{\rho\nu}{4\sigma_0} (x - k) + \frac{\nu^2}{24\sigma_0^3} (x - k)^2. \quad (2.3)$$

For an ATM European call option far away from maturity ($T \rightarrow \infty$), the following holds:

$$I(T, K) \approx \sqrt{\theta} \left(1 + \frac{\nu\rho}{4\kappa} - \frac{\nu^2}{32\kappa^2} \right) + \left(\frac{\sigma_0^2 - \theta}{2\kappa\sqrt{\theta}} + \nu\rho \frac{\sigma_0^2 - 2\theta}{4\kappa^2\sqrt{\theta}} - \nu^2 \frac{\sigma_0^2 - \frac{5}{2}\theta + 4\kappa}{32\sqrt{\theta}\kappa^3} \right) \frac{1}{T}. \quad (2.4)$$

When the option is at-the-money ($x = k - rT$), the expansion around σ_0 is:

$$I(T, K) \approx \sigma_0 + \frac{3\sigma_0^2\rho\nu - 6\kappa(\sigma_0^2 - \theta) - \nu^2}{24\sigma_0} T. \quad (2.5)$$

To calibrate the parameters, the above approximations are used in the following way:

- A linear equation is fitted to the ATM implied volatilities for different values of T . The values of σ_0 and

$$\frac{3\sigma_0^2\rho\nu - 6\kappa(\sigma_0^2 - \theta) - \nu^2}{24\sigma_0}$$

are obtained from (2.5).

- A linear equation is fitted to the implied volatilities for short maturities as a function of the log-moneyness ($x - k$). Equation (2.3) provides the value of $\rho\nu$. Notice that for strikes close to the money, the linear component is stronger than the curvature, making it difficult to estimate ν directly.
- For large values of T an equation is fitted to the implied volatilities as a function of $1/T$. The values of

$$\sqrt{\theta} \left(1 + \frac{\nu\rho}{4\kappa} - \frac{\nu^2}{32\kappa^2} \right)$$

and

$$\left(\frac{\sigma_0^2 - \theta}{2\kappa\sqrt{\theta}} + \nu\rho \frac{\sigma_0^2 - 2\theta}{4\kappa^2\sqrt{\theta}} - \nu^2 \frac{\sigma_0^2 - \frac{5}{2}\theta + 4\kappa}{32\sqrt{\theta}\kappa^3} \right).$$

are then obtained from (2.4).

- The previous steps provide a system of three equations. By solving them, the full set of Heston parameters $(\sigma_0, \nu, \kappa, \theta, \rho)$ is calibrated.

The numerical examples in Alòs et al. (2015) are quite accurate and will be used in Section 5 as the benchmark against which the results from the signature-based model will be measured. A drawback of this method, however, lies in the assumption of taking the Heston model as the underlying dynamics for the volatility process. As a result, its flexibility is constrained by the limitations of that specific model, which may not adequately capture roughness or other complex behaviors observed in real markets.

In Section 4 we introduce a data-driven model based on path signatures, which does not assume any specific parametric form for the volatility process. Instead of presupposing a Heston-type dynamics, this approach can learn directly from a *primary* noise, enabling it to adapt to a broader class of behaviors. This added flexibility makes the signature-based model a compelling alternative for capturing the full richness of empirical volatility patterns.

3 Path Signatures

A natural way to incorporate signatures into stochastic volatility modeling is through the framework proposed by Cuchiero et al. (2023), where the *asset price* is modeled as a linear functional of the signature of a driving noise process. Although this approach performs well under the assumption that the volatility process is a semimartingale, it is less suitable in settings characterized by rough volatility, where such regularity assumptions no longer hold.

To address this limitation, Cuchiero et al. (2025) propose an alternative formulation in which the *volatility* process itself is expressed as a linear functional of the signature of the primary noise. Although this approach is computationally more intensive, it does not require the volatility to satisfy any martingale or semimartingale condition, making it particularly well-suited to the modeling of rough or highly irregular volatility dynamics.

In this paper, we adopt a similar approach, that is, we assume that the volatility is a continuous function of a general underlying stochastic process, called the *primary noise*, which does not need to be of the Heston type. This continuous function is then approximated by a linear combination of the elements of the signature of the primary noise.

We now introduce the essential ideas from rough path theory underpinning our signature-based approach. We include some proofs to support intuition. For a comprehensive treatment of rough paths, we refer to Chevyrev and Kormilitzin (2016), Cuchiero et al. (2023), and Lyons and Qian (2002). Insightful and clear expositions are given in Geng (2021) and Díaz (2023), which we follow in several places.

The need for signatures arises from the problem of defining integrals of the form

$$\int_s^t y_u dx_u \tag{3.1}$$

when the integrand y and integrator x lack sufficient regularity. If both x and y have bounded variation, the integral is defined in the Riemann–Stieltjes or Lebesgue–Stieltjes sense. If x and y are α -Hölder continuous with $\alpha > \frac{1}{2}$, Young’s theory applies. However, when $\alpha \leq \frac{1}{2}$, classical constructions break down, and the Riemann sums

$$\sum_{t_i \in \mathcal{D}} y_{t_{i-1}} (x_{t_i} - x_{t_{i-1}})$$

may fail to converge as the mesh $|\mathcal{D}| \rightarrow 0$. At best, these sums provide a first-order approximation to the integral, and additional structure is needed to make sense of the limit.

Note that these approximations depend only on the increments $x_t - x_s$. In fact, the *first level of the signature* of a path x corresponds precisely to its increments. The signature can then be understood as an enhanced path that augments its first-order increments with higher-order information in the form of *iterated integrals*.

To illustrate why higher-order terms are essential, we use the following example from Geng (2021). Consider a smooth function F and let $y_t = F(x_t)$. Then, formally, one can write:

$$\begin{aligned} \int_s^t F(x_u) dx_u &= F(x_s)(x_t - x_s) + \int_s^t (F(x_u) - F(x_s)) dx_u \\ &= F(x_s)(x_t - x_s) + \int_s^t \int_s^u DF(x_v) dx_v dx_u \\ &= F(x_s)(x_t - x_s) + DF(x_s) \int_s^t \int_s^u dx_v dx_u \\ &\quad + \int_s^t \int_s^u (DF(x_v) - DF(x_s)) dx_v dx_u. \end{aligned}$$

Continuing recursively leads to the formal expansion

$$\begin{aligned} \int_s^t F(x_u) dx_u &= F(x_s)(x_t - x_s) + DF(x_s) \int_s^t \int_s^u dx_v dx_u \\ &\quad + D^2 F(x_s) \int_s^t \int_s^u \int_s^v dx_r dx_v dx_u \\ &\quad + D^3 F(x_s) \int_s^t \int_s^u \int_s^v \int_s^r dx_z dx_r dx_v dx_u + \dots \end{aligned}$$

That is, computing the integral $\int_s^t F(x_u) dx_u$ requires access to a full collection of iterated integrals of x , not just its increments.

Note that if x takes values in \mathbb{R}^d , then the second-level iterated integral

$$\int_s^t \int_s^u dx_v dx_u$$

is a tensor consisting of d^2 terms of the form $\int_s^t \int_s^u dx_v^i dx_u^j$. Higher-order levels live in higher tensor powers. Thus, the natural way to organize this structure is through the *tensor algebra*, introduced formally below.

In low regularity settings (like Brownian motion or rough volatility models), these higher-order iterated integrals are not well-defined. Rough path theory allows us to *define* them abstractly, thereby extending integration to paths of low regularity.

Informally, if x is α -Hölder continuous, we expect that

$$\left| \int_{s < t_1 < \dots < t_n < t} dx_{t_1} \cdots dx_{t_n} \right| \lesssim |t - s|^{n\alpha},$$

so higher-order terms decay rapidly. This motivates approximating the integral of a function $F(x_t)$ against dx_t as

$$\int_s^t F(x_u) dx_u \approx \sum_{k=1}^N DF^{(k-1)}(x_s) \mathbf{X}_{s,t}^k,$$

where $\mathbf{X}_{s,t}^k = \int_{s < t_1 < \dots < t_k < t} dx_{t_1} \cdots dx_{t_k}$ will represent the k -th level of the signature of x . The truncation level N will depend on the regularity of x .

As a result, to define pathwise integration in irregular settings, and to model functionals of paths (such as volatility), we must specify a family of tensors $(\mathbf{X}_{s,t}^k)_{k=1}^N$ satisfying some algebraic and analytic constraints. These will form the signature of a rough path, which we now formalize by introducing the tensor algebra.

3.1 Tensor Algebras

Let V be a real-valued finite dimensional vector space. In practice, V will typically be \mathbb{R}^d , for some $d \geq 1$. For any non-negative integer n , we denote the n -th tensor power of V as

$$V^{\otimes n} := V \otimes \cdots \otimes V,$$

with $V^{\otimes 0} = \mathbb{R}$. The tensor power of a vector space is a vector space as well. Moreover, if V is isomorphic to \mathbb{R}^d for some $d \geq 1$ then $V^{\otimes n}$ is isomorphic to \mathbb{R}^{d^n} . In particular, all tensor powers of \mathbb{R} are isomorphic to \mathbb{R} itself.

If e_1, \dots, e_d is a basis of V , then the elements $\{e_{i_1} \otimes \cdots \otimes e_{i_n}; (i_1, \dots, i_n) \in \{1, \dots, d\}^n\}$ are a basis of $V^{\otimes n}$, that is, every tensor $v \in V^{\otimes n}$ can be written uniquely as

$$v = \sum_{1 \leq i_1, \dots, i_n \leq d} \lambda_{i_1, \dots, i_n} e_{i_1} \otimes \cdots \otimes e_{i_n},$$

for some coefficients $\{\lambda_{i_1, \dots, i_n} \in \mathbb{R}; (i_1, \dots, i_n) \in \{1, \dots, d\}^n\}$.

Definition 3.1 (Extended Tensor Algebra). *We define the extended tensor algebra $T((V))$ over V as the set*

$$T((V)) = \{\mathbf{a} = (a_0, a_1, \dots); a_n \in V^{\otimes n}\}$$

equipped with the following element-wise addition and scalar product

$$\mathbf{a} + \mathbf{b} = (a_0 + b_0, \dots, a_n + b_n, \dots), \quad \lambda \mathbf{a} = (\lambda a_0, \lambda a_1, \dots),$$

and endowed with the product \otimes defined by

$$\mathbf{a} \otimes \mathbf{b} = (c_0, c_1, \dots),$$

where

$$c_n = \sum_{i+j=n} a_i \otimes b_j.$$

In the same way that we can define a product in $T((V))$, we can characterize its invertible elements. Specifically, if $\mathbf{a} \in T((V))$ and the zeroth level $a_0 \in \mathbb{R}$ is nonzero, then \mathbf{a} admits a multiplicative inverse in $T((V))$, given by the formal series:

$$\mathbf{a}^{-1} = \sum_{n \geq 0} \frac{1}{a_0} \left(\mathbf{1} - \frac{\mathbf{a}}{a_0} \right)^{\otimes n},$$

where $\mathbf{1} := (1, 0, 0, \dots)$ is the multiplicative identity in $T((V))$, and the powers are taken with respect to the tensor product. Finally, we define the tensor algebra over V as the set

$$T(V) = \{\mathbf{a} \in T((V)); \exists n \in \mathbb{N} \text{ such that } a_k = 0 \ \forall k \geq n\}.$$

In other words, $T(V)$ consists of all formal tensor series with only finitely many nonzero terms.

To make the notation more concise, define the multi-index $I = (i_1, \dots, i_n) \in \{1, \dots, d\}^n$. We then write $e_I = e_{i_1} \otimes \dots \otimes e_{i_n}$, and we denote the length of I by $|I| = n$. In order to write scalars, we set $\alpha = \alpha e_\emptyset$, with $|\emptyset| = 0$. This notation allows us to write any tensor $v \in V^{\otimes n}$ as

$$v = \sum_{|I|=n} \lambda_I e_I,$$

for some coefficients $\{\lambda_I \in \mathbb{R}; |I| = n\}$.

Given an element of $T(V)$, we can naturally associate a linear map on $T((V))$, in a manner analogous to the Riesz representation Theorem.

Definition 3.2. *For any $\ell = \sum_{|I| \geq 0} \ell_I e_I \in T(V)$ and $\mathbf{a} = \sum_{|I| \geq 0} a_I e_I \in T((V))$, we define the map $\langle \cdot, \cdot \rangle : T(V) \times T((V)) \rightarrow \mathbb{R}$ by*

$$\langle \ell, \mathbf{a} \rangle := \sum_{|I| \geq 0} \ell_I a_I. \quad (3.2)$$

This map is well defined because there are only finitely many nonzero elements ℓ_I . Note that we can recover the coordinate a_I of \mathbf{a} with $\langle e_I, \mathbf{a} \rangle = a_I$.

We now introduce another important product on $T(V)$. The shuffle product is a way to combine two tensors in $T(V)$ by interweaving their entries in all possible ways, while *preserving the relative order* within each tensor. Its effect is usually compared to that of shuffling cards from two decks while keeping each deck's internal order intact. The shuffle product is important in rough path theory because it encodes how products of iterated integrals combine.

Definition 3.3. *For any multi-indices $I = (i_1, \dots, i_n)$ and $J = (j_1, \dots, j_m)$, let $I' = (i_1, \dots, i_{n-1})$ and $J' = (j_1, \dots, j_{m-1})$. The shuffle product $e_I \sqcup e_J$ is defined recursively as*

$$e_I \sqcup e_J = (e_{I'} \sqcup e_J) \otimes e_{i_n} + (e_I \sqcup e_{J'}) \otimes e_{j_m},$$

with the convention $e_I \sqcup e_\emptyset = e_\emptyset \sqcup e_I = e_I$.

Example 3.4. If we consider $e_1 \otimes e_2$ and e_3 we get

$$(e_1 \otimes e_2) \sqcup e_3 = e_1 \otimes e_3 \otimes e_2 + e_3 \otimes e_1 \otimes e_2 + e_1 \otimes e_2 \otimes e_3.$$

The shuffle product of two tensors of lengths m and n has $\binom{m+n}{m}$ elements.

Example 3.5. Consider $I = \{1, 2, 3\}$ and $J = \{2, 1\}$. With a slight abuse of notation, we may write $e_I = e_1 \otimes e_2 \otimes e_3 = e_{123}$ and $e_J = e_2 \otimes e_1 = e_{21}$. To better observe the shuffling, in the expression below we underline the indexes corresponding to e_{21} :

$$\begin{aligned} e_{123} \sqcup e_{21} &= e_{123\underline{21}} + e_{\underline{21}23} + e_{2\underline{1}123} + e_{21\underline{1}23} + e_{212\underline{1}3} \\ &\quad + e_{1\underline{2}23\underline{1}} + e_{1\underline{2}2\underline{1}3} + e_{1\underline{2}1\underline{2}3} + e_{1\underline{2}23\underline{1}} + e_{1\underline{2}2\underline{1}3} \\ &= e_{12321} + e_{12123} + 2e_{12213} + 2e_{12231} + 2e_{21123} + e_{21213} + e_{21231}. \end{aligned}$$

While $e_1 \otimes e_2 \otimes e_3 \in V^{\otimes 3}$ and $e_2 \otimes e_1 \in V^{\otimes 2}$, note that $e_1 \otimes e_2 \otimes e_3 \sqcup e_2 \otimes e_1 \in V^{\otimes 5}$. As we will see in Section 4.1, the shuffle product sharply increases the order of computations required to construct our signature-based approximation to the volatility.

Let $\ell^1, \ell^2 \in T(V)$, with $\ell^1 = \sum_{|I| \geq 0} \ell_I^1 e_I$ and $\ell^2 = \sum_{|J| \geq 0} \ell_J^2 e_J$. We then have:

$$\ell^1 \sqcup \ell^2 = \sum_{|I|, |J| \geq 0} \ell_I^1 \ell_J^2 e_I \sqcup e_J.$$

The collection $(T(V), +, \cdot, \sqcup)$ is a commutative algebra.

3.2 Signature of Paths of Bounded Variation

We say that $\mathcal{D}_{[0, T]} = \{t_0, t_1, \dots, t_n\}$ is a partition of the interval $[0, T]$ if $0 = t_0 < t_1 < \dots < t_n = T$. If the interval is clear from the context, we will simply write \mathcal{D} . Let V be a d -dimensional vector space.

Definition 3.6. Let $p \geq 1$. A continuous path $X : [0, T] \rightarrow V$ has finite p -variation in $[0, T]$ if

$$\|X\|_p = \left(\sup_{\mathcal{D}} \sum_{t_i \in \mathcal{D}} |X_{t_{i+1}} - X_{t_i}|^p \right)^{1/p}$$

is finite. We denote by $\mathcal{V}^p([0, T])$ the set of continuous paths with finite p -variation in $[0, T]$.

It is not difficult to show that if $1 < p < q$, then

$$\mathcal{V}^1([0, T]) \subset \mathcal{V}^p([0, T]) \subset \mathcal{V}^q([0, T]) \subset \mathcal{C}([0, T]).$$

If $X \in \mathcal{V}^1([0, T])$, we say that X is of bounded variation.

To define the signature of a continuous path of bounded variation, we need to define integrals with respect to paths. Notice that, since X has bounded variation, one can define the integral with respect to X using Young's integration theory (see Young (1936)).

Definition 3.7 (Signature). Consider a d -dimensional vector space V and let $X : [0, T] \rightarrow V$ be a continuous path of bounded variation. Using the multi-index notation $I = (i_1, \dots, i_n) \in \{1, \dots, d\}^n$, we define the signature of X on the interval $[0, T]$ as

$$S(X)_{0, T} = \sum_{|I| \geq 0} S(X)_{0, T}^I e_I,$$

where the coefficients of the signature are defined recursively as

$$\begin{aligned} S(X)_{0, T}^0 &= \langle e_\emptyset, S(X)_{0, T} \rangle := 1 \\ S(X)_{0, T}^I &= \langle e_I, S(X)_{0, T} \rangle := \int_0^T \langle e_I, S(X)_{0, s} \rangle dX_s^{i_n}. \end{aligned}$$

Recall that $I' = (i_1, \dots, i_{n-1})$. The element of the signature corresponding to index I can be written as

$$S(X)_{0,T}^{i_1, \dots, i_n} = \int_{0 < s_1 < \dots < s_n < T} dX_{s_1}^{i_1} \dots dX_{s_n}^{i_n}.$$

To gain some insight into the structure of the signature, consider the following two examples from Chevyrev and Kormilitzin (2016).

Example 3.8. Consider a one-dimensional path $X : [0, t] \rightarrow \mathbb{R}$. In this case, the multi-indexes are $I = (i_1, \dots, i_n) \in \{1\}^n$. The signature of X is then given by

$$\begin{aligned} S(X)_{0,t}^0 &= 1 \\ S(X)_{0,t}^1 &= \int_0^t dX_s = X_t - X_0 \\ S(X)_{0,t}^{11} &= \int_0^t \int_0^s dX_u dX_s = \frac{1}{2!} (X_t - X_0)^2 \\ S(X)_{0,t}^{111} &= \int_0^t \int_0^s \int_0^u dX_r dX_u dX_s = \frac{1}{3!} (X_t - X_0)^3 \end{aligned}$$

and so on.

Example 3.9. Let $X : [0, 5] \rightarrow \mathbb{R}^2$ be defined by $X_t = (X_t^1, X_t^2) = (3 + t, (3 + t)^2)$. Being a two-dimensional path, the multi-indexes are $I = (i_1, \dots, i_n) \in \{1, 2\}^n$. The elements of the signature are

$$\begin{aligned} S(X)_{0,5}^0 &= 1 \\ S(X)_{0,5}^1 &= \int_0^5 dX_t^1 = \int_0^5 dt = X_5^1 - X_0^1 = 5 \\ S(X)_{0,5}^2 &= \int_0^5 dX_t^2 = \int_0^5 2(3 + t)dt = X_5^2 - X_0^2 = 55 \\ S(X)_{0,5}^{11} &= \int_0^5 \int_0^t dX_s^1 dX_t^1 = \int_0^5 \left[\int_0^t ds \right] dt = \frac{25}{2} \\ S(X)_{0,5}^{12} &= \int_0^5 \int_0^t dX_s^1 dX_t^2 = \int_0^5 \left[\int_0^t ds \right] 2(3 + t)dt = \frac{475}{3} \\ S(X)_{0,5}^{21} &= \int_0^5 \int_0^t dX_s^2 dX_t^1 = \int_0^5 \left[\int_0^t 2(3 + s)ds \right] dt = \frac{350}{3} \\ S(X)_{0,5}^{22} &= \int_0^5 \int_0^t dX_s^2 dX_t^2 = \int_0^5 \left[\int_0^t 2(3 + s)ds \right] 2(3 + t)dt = \frac{3025}{2} \\ S(X)_{0,5}^{111} &= \int_0^5 \int_0^t \int_0^s dX_u^1 dX_s^1 dX_t^1 = \int_0^5 \left[\int_0^t \left[\int_0^s du \right] ds \right] dt = \frac{125}{6} \end{aligned}$$

and so on. The signature of X on $[0, 5]$ can therefore be written as

$$S(X)_{0,5} = (1, 5, 55, 12.5, 158.33, 116.66, 1512.5, 20.83, \dots).$$

The next result, known as Chen's identity, shows that, even though a path's signature is defined algebraically, it still captures the way the path evolves over time. In particular, it enables the reconstruction of the signature of X over the interval $[0, T]$ provided that it is known on a collection of subintervals that cover $[0, T]$.

Theorem 3.10 (Chen's identity). *Let $X : [0, T] \rightarrow V$ be a continuous path of bounded variation. Then, for all $t \in (0, T)$,*

$$S(X)_{0,T} = S(X)_{0,t} \otimes S(X)_{t,T}. \quad (3.3)$$

Proof. We need to prove that, given i_1, \dots, i_n , then

$$S(X)_{0,T}^{i_1, \dots, i_n} = \sum_{k=0}^n S(X)_{0,t}^{i_1, \dots, i_k} S(X)_{t,T}^{i_{k+1}, \dots, i_n}$$

We use induction on the level of signature n . If $n = 0$ then (3.3) is simply

$$1 = 1 \otimes 1,$$

which holds trivially. Assume that (3.3) holds for all $n \geq 0$. For $n + 1$ we have

$$\begin{aligned} S(X)_{0,T}^{i_1, \dots, i_{n+1}} &= \int_0^T S(X)_{0,s}^{i_1, \dots, i_n} dX_s^{i_{n+1}} \\ &= \int_0^t S(X)_{0,s}^{i_1, \dots, i_n} dX_s^{i_{n+1}} + \int_t^T S(X)_{0,s}^{i_1, \dots, i_n} dX_s^{i_{n+1}} \\ &= S(X)_{0,t}^{i_1, \dots, i_{n+1}} + \int_t^T S(X)_{0,s}^{i_1, \dots, i_n} dX_s^{i_{n+1}} \\ &= S(X)_{0,t}^{i_1, \dots, i_{n+1}} + \int_t^T \sum_{k=0}^n S(X)_{0,t}^{i_1, \dots, i_k} S(X)_{t,s}^{i_{k+1}, \dots, i_n} dX_s^{i_{n+1}}, \end{aligned}$$

where the last equality follows from the induction step. Rearranging,

$$\begin{aligned} S(X)_{0,T}^{i_1, \dots, i_{n+1}} &= S(X)_{0,t}^{i_1, \dots, i_{n+1}} + \sum_{k=0}^n S(X)_{0,t}^{i_1, \dots, i_k} \int_t^T S(X)_{t,s}^{i_{k+1}, \dots, i_n} dX_s^{i_{n+1}} \\ &= S(X)_{0,t}^{i_1, \dots, i_{n+1}} + \sum_{k=0}^n S(X)_{0,t}^{i_1, \dots, i_k} S(X)_{t,T}^{i_{k+1}, \dots, i_{n+1}} \\ &= \sum_{k=0}^{n+1} S(X)_{0,t}^{i_1, \dots, i_k} S(X)_{t,T}^{i_{k+1}, \dots, i_{n+1}}. \end{aligned}$$

which concludes the proof. \square

From the definition of the signature, it is clear that $S(X)_{0,T} \in T((V))$. However, we can show that the signature of X lies in a smaller space.

Definition 3.11. An element $\mathbf{a} \in T((V))$ is said to be group-like if for every pair $\ell^1, \ell^2 \in T(V)$ we have

$$\langle \ell^1, \mathbf{a} \rangle \langle \ell^2, \mathbf{a} \rangle = \langle \ell^1 \sqcup \ell^2, \mathbf{a} \rangle.$$

We denote by $G(V)$ the set of group-like elements of $T((V))$.

The group-like property is *analogous* to the behavior of exponentials: just as $e^{x+y} = e^x e^y$ transforms addition into multiplication, signatures can be thought of as “exponentials” of paths rather than numbers. The shuffle product represents all the ways in which two tensors (say, ℓ_1 and ℓ_2) can be combined while preserving their internal order. The group-like condition says that evaluating the shuffle is equivalent to evaluating each tensor separately and multiplying the results. We now make this idea precise.

Proposition 3.12. Let $X : [0, T] \rightarrow V$ be a continuous path of bounded variation. Then, the signature of X satisfies the group-like property. That is, for every pair $\ell^1, \ell^2 \in T(V)$,

$$\langle \ell^1, S(X)_{0,T} \rangle \langle \ell^2, S(X)_{0,T} \rangle = \langle \ell^1 \sqcup \ell^2, S(X)_{0,T} \rangle.$$

Proof. By linearity, it is enough to prove it for $\ell^1 = e_I$ and $\ell^2 = e_J$. Let $n = |I| + |J|$. We will prove the result by induction on n . For $n = 0$, we have $I = J = \emptyset$ and the result holds trivially. Assume that it holds for n , and let $I = (i_1, \dots, i_{n+1-m})$ and $J = (j_1, \dots, j_m)$. Note first

that $\langle e_I, S(X)_{0,T} \rangle = S(X)_{0,T}^I$ and $\langle e_J, S(X)_{0,T} \rangle = S(X)_{0,T}^J$. Using integration by parts and the notation for I' and J' introduced in Definition 3.3, we have

$$\begin{aligned} & \langle e_I, S(X)_{0,T} \rangle \langle e_J, S(X)_{0,T} \rangle \\ &= \int_0^T \langle e_J, S(X)_{0,s} \rangle d\langle e_I, S(X)_{0,s} \rangle + \int_0^T \langle e_I, S(X)_{0,s} \rangle d\langle e_J, S(X)_{0,s} \rangle \\ &= \int_0^T \langle e_{I'}, S(X)_{0,s} \rangle \langle e_J, S(X)_{0,s} \rangle dX_s^{i_{n+1}-m} + \int_0^T \langle e_I, S(X)_{0,s} \rangle \langle e_{J'}, S(X)_{0,s} \rangle dX_s^{j_m}. \end{aligned}$$

Using the induction step, it follows that

$$\begin{aligned} & \langle e_I, S(X)_{0,T} \rangle \langle e_J, S(X)_{0,T} \rangle \\ &= \int_0^T \langle (e_{I'} \sqcup e_J), S(X)_{0,s} \rangle dX_s^{i_{n+1}-m} + \int_0^T \langle (e_I \sqcup e_{J'}), S(X)_{0,s} \rangle dX_s^{j_m} \\ &= \langle (e_{I'} \sqcup e_J) \otimes e_{n+1-m}, S(X)_{0,T} \rangle + \langle (e_I \sqcup e_{J'}) \otimes e_{j_m}, S(X)_{0,T} \rangle \\ &= \langle (e_I \sqcup e_J), S(X)_{0,T} \rangle, \end{aligned}$$

which concludes the proof. \square

The function $\langle \cdot, \cdot \rangle$ defined in (3.2) allows us to interpret the elements ℓ of the tensor algebra $T(V)$ as linear functionals when paired with a signature $S(X)_{0,T}$. If we evaluate two linear functionals ℓ_1 and ℓ_2 separately on the signature $S(X)_{0,T}$ and then multiply those two scalar values, that product equals what we get by evaluating the single functional $\ell^1 \sqcup \ell^2$ on $S(X)_{0,T}$.

If we consider the path $X : [0, 5] \rightarrow \mathbb{R}^2$ from Example 3.9, we have

$$S(X)_{0,5}^{12} = \int_0^5 \int_0^t dX_s^1 dX_t^2 \quad \text{and} \quad S(X)_{0,5}^1 = \int_0^5 dX_t^1.$$

The multiplication of these two iterated integrals would be a polynomial in the components of the signature $S(X)_{0,T}$. The above proposition says that such a nonlinear expression can still be treated in a linear way provided we use the shuffle product. With the slight abuse of notation used in Example 3.5, we see that $e_{12} \sqcup e_1 = e_{121} + 2e_{112}$. Therefore, the product of the iterated integrals $S(X)_{0,5}^{12}$ and $S(X)_{0,5}^1$ can be expressed as a linear combination of

$$S(X)_{0,5}^{121} = \int_0^5 \int_0^t \int_0^s dX_u^1 dX_s^2 dX_t^1 \quad \text{and} \quad S(X)_{0,5}^{112} = \int_0^5 \int_0^t \int_0^s dX_u^1 dX_s^1 dX_t^2.$$

In other words, products of iterated integrals (polynomials in the elements of the signature) can be written as linear combinations of *higher-order* integrals. The fact that the space of polynomials on signatures can be linearly organized via the shuffle product will be used in Section 4. The price to pay for linearity is the higher dimension of the tensor space in which the linear expression lives, which happens to be the space in which numerical computations will be carried out.

3.3 Rough Paths

So far we have developed the signature for continuous paths of bounded variation. By Young's integration theory, this construction extends to continuous paths of finite p -variation for $p < 2$. However, the stochastic processes most commonly used in finance—such as Brownian motion or fractional Brownian motion with small Hurst indexes—do not satisfy this condition. We therefore need to find a way to extend the signature to a broader class of paths with more irregular behavior.

This extension is achieved by *lifting* the paths. Intuitively, *lifting* refers to the process of enriching a path with additional information (namely, its iterated integrals).

Let $X : [0, T] \rightarrow V$ be a path of finite p -variation for some $p \geq 2$, so that X may be too irregular for classical iterated integrals to exist. To overcome this difficulty, we define a new object called a rough path

$$\mathbf{X}_{s,t} = \left(\mathbb{X}_{s,t}^1, \mathbb{X}_{s,t}^2, \mathbb{X}_{s,t}^3, \dots, \mathbb{X}_{s,t}^{[p]} \right),$$

where $\mathbb{X}_{s,t}^1 = X_t - X_s$ is the increment of the original path and each $\mathbb{X}_{s,t}^k$ is an approximation to the k -th order iterated integral

$$\mathbb{X}_{s,t}^k \approx \int_{s < u_1 < \dots < u_k < t} dX_{u_1} \otimes \dots \otimes dX_{u_k}$$

At this level of intuition, *approximation* means that the \mathbb{X}^k serve as surrogates for the true iterated integrals, satisfying algebraic properties like Chen's identity and appropriate p -variation bounds. This lifted structure enables us to define integration against X even when classical approaches such as Riemann–Stieltjes or Young integration break down. In the remainder of this section we formalize these ideas.

Definition 3.13 (Truncated Tensor Algebra). *Let $N \in \mathbb{N}$. We define the truncated tensor algebra of order N over V as*

$$T^N(V) = \{\mathbf{a} = (a_0, a_1, \dots) \in T((V)); a_k = 0 \ \forall k > N\}.$$

The projection map $\pi_{\leq N} : T((V)) \rightarrow T^N(V)$ is defined as

$$\pi_{\leq N}((a_i)_{i=0}^\infty) = (a_i)_{i=0}^N.$$

For any $\mathbf{a}, \mathbf{b} \in T^N(V)$, we define the truncated tensor product in $T^N(V)$ as

$$\mathbf{a} \otimes_{\leq N} \mathbf{b} = \pi_{\leq N}(\mathbf{a} \otimes \mathbf{b}).$$

When dealing with elements of $T^N(V)$, if there is no risk of confusion we will generally use \otimes to denote $\otimes_{\leq N}$.

Let $X : [0, T] \rightarrow V$ be a continuous path of bounded variation and $\Delta_T = \{(s, t) \in [0, T]^2; s \leq t\}$. The truncated signature of order N of a path X can therefore be defined as

$$\begin{aligned} S(X)^{\leq N} : \Delta_T &\rightarrow T^N(V) \\ (s, t) &\mapsto \pi_{\leq N}(S(X)_{s,t}). \end{aligned}$$

We write $S(X)^{\leq N}(s, t) = S(X)_{s,t}^{\leq N}$.

A slight modification in the proof of Chen's identity shows that, for all $0 \leq s < u < t \leq T$,

$$S(X)_{s,t}^{\leq N} = S(X)_{s,u}^{\leq N} \otimes S(X)_{u,t}^{\leq N}. \quad (3.4)$$

We say that $S(X)^{\leq N}$ is *multiplicative*. The following definition extends the multiplicative property to a more general setting.

Definition 3.14 (Multiplicative functional). *For $N \in \mathbb{N}$, let $\mathbf{X} : \Delta_T \rightarrow T^N(V)$ be a continuous map and denote $\mathbf{X}(s, t) = \mathbf{X}_{s,t}$. Since $\mathbf{X}_{s,t} \in T^N(V)$, we can write $\mathbf{X}_{s,t} = (\mathbf{X}_{s,t}^0, \mathbf{X}_{s,t}^1, \dots, \mathbf{X}_{s,t}^N)$, where $\mathbf{X}_{s,t}^k \in V^{\otimes k}$ for each k . We say that \mathbf{X} is a multiplicative functional of degree N in V if, for every $(s, t) \in \Delta_T$, we have $\mathbf{X}_{s,t}^0 := 1$ and*

$$\mathbf{X}_{s,t} = \mathbf{X}_{s,u} \otimes \mathbf{X}_{u,t} \quad (3.5)$$

for all $s \leq u \leq t$.

By extension, we also refer to (3.5) as Chen's identity. Consider the case when $N = 1$. Chen's identity says that

$$(1, \mathbf{X}_{s,t}^1) = (1, \mathbf{X}_{s,u}^1) \otimes (1, \mathbf{X}_{u,t}^1) = (1, \mathbf{X}_{s,u}^1 + \mathbf{X}_{u,t}^1),$$

which implies $\mathbf{X}_{s,t}^1 = \mathbf{X}_{s,u}^1 + \mathbf{X}_{u,t}^1$. The type of functionals that satisfy this property are called *additive functionals*. Additivity provides an important step toward the definition of a rough path.

Select an arbitrary constant $v \in V$ and define a path $\psi : [0, T] \rightarrow V$ by

$$\psi_t := v + \mathbf{X}_{0,t}^1.$$

Then, $\psi_t - \psi_s = \mathbf{X}_{0,t}^1 - \mathbf{X}_{0,s}^1$. By additivity (Chen's identity at level 1), this equals $\mathbf{X}_{s,t}^1$. That is,

$$\mathbf{X}_{s,t}^1 = \psi_t - \psi_s.$$

In other words, a multiplicative functional of order 1 in V is equivalent to the increment map of a path $\psi : [0, T] \rightarrow V$, unique up to an additive constant.

Up to now, we started from a continuous path of finite variation $X : [0, T] \rightarrow V$ and showed that its truncated signature—an element of the tensor algebra $T^N(V)$ —satisfies the multiplicative identity (3.4). We now reverse this perspective: instead of constructing the signature from a classical path, we assume the algebraic structure of a signature and study its properties as a path taking values in the tensor algebra $T^N(V)$.

We have already seen that the first level of a multiplicative functional is given by the increments of a path in V , just as the first level of the signature of a path corresponds to its own increments. We can now generalize this.

Lemma 3.15. *Let $\mathbf{X}, \mathbf{Y} : \Delta_T \rightarrow T^N(V)$ be two multiplicative functionals of order N that agree on the first $N - 1$ levels. Then, the function $\Psi : \Delta_T \rightarrow V^{\otimes N}$ defined by $\Psi_{s,t} = \mathbf{X}_{s,t}^N - \mathbf{Y}_{s,t}^N$ is additive, that is, $\Psi_{s,t} = \Psi_{s,u} + \Psi_{u,t}$, for all $s \leq u \leq t$.*

Proof. Due to the multiplicative property, $\mathbf{X}_{s,t} = \mathbf{X}_{s,u} \otimes \mathbf{X}_{u,t}$ for all $s \leq u \leq t$. Consider the N -th level component of the functionals in each side of the last equality. In the case of the N -th level component of $\mathbf{X}_{s,u} \otimes \mathbf{X}_{u,t}$, we separate the summands that only include elements of $V^{\otimes N}$ from the rest, which are tensor products of elements from lower levels:

$$\mathbf{X}_{s,t}^N = \mathbf{X}_{s,u}^N + \mathbf{X}_{u,t}^N + \sum_{i+j=N-1} \mathbf{X}_{s,u}^i \otimes \mathbf{X}_{u,t}^j.$$

An analogous expression holds for $\mathbf{Y}_{s,t}^N$. Then,

$$\Psi_{s,t} = \mathbf{X}_{s,t}^N - \mathbf{Y}_{s,t}^N = \Psi_{s,u} + \Psi_{u,t} + \sum_{i+j=N-1} \left(\mathbf{X}_{s,u}^i \otimes \mathbf{X}_{u,t}^j - \mathbf{Y}_{s,u}^i \otimes \mathbf{Y}_{u,t}^j \right).$$

As \mathbf{X} and \mathbf{Y} agree on the first $N - 1$ levels, the last term on the right-hand side is zero, yielding $\Psi_{s,t} = \Psi_{s,u} + \Psi_{u,t}$, which is what we needed to prove. \square

Lemma 3.16. *Let $\mathbf{X} : \Delta_T \rightarrow T^N(V)$ be a multiplicative functional of order N in V and let $\Psi : \Delta_T \rightarrow V^{\otimes N}$ be an additive function. Then $\mathbf{X}_{s,t} + \Psi_{s,t}$ is also a multiplicative functional.*

Proof. We need to show that, for all $s \leq u \leq t$,

$$\mathbf{X}_{s,t} + \Psi_{s,t} = (\mathbf{X}_{s,u} + \Psi_{s,u}) \otimes (\mathbf{X}_{u,t} + \Psi_{u,t}).$$

The right hand side of the above expression can be expanded as

$$\mathbf{X}_{s,u} \otimes \mathbf{X}_{u,t} + \mathbf{X}_{s,u} \otimes \Psi_{u,t} + \Psi_{s,u} \otimes \mathbf{X}_{u,t} + \Psi_{s,u} \otimes \Psi_{u,t}.$$

As \mathbf{X} is multiplicative, $\mathbf{X}_{s,u} \otimes \mathbf{X}_{u,t} = \mathbf{X}_{s,t}$. We now prove that

$$\mathbf{X}_{s,u} \otimes \Psi_{u,t} + \Psi_{s,u} \otimes \mathbf{X}_{u,t} + \Psi_{s,u} \otimes \Psi_{u,t} = \Psi_{s,t}. \quad (3.6)$$

Note that Ψ takes values in $V^{\otimes N}$, which is the highest order component in the truncated tensor algebra $T^N(V)$. Therefore, when tensoring $\mathbf{X}_{s,u}$ with $\Psi_{u,t}$, the only element in $V^{\otimes N}$ will be

precisely $\Psi_{u,t}$. That is, $\mathbf{X}_{s,u} \otimes_{\leq N} \Psi_{u,t} = \Psi_{u,t}$. More formally, assume that $\mathbf{X}_{s,u} = \sum_{|J| \leq N} b_J e_J$ for some coefficients b_J , and let $I = (0, \dots, 0, 1)$ with $|I| = N$. Then, as $b_\emptyset = 1$,

$$\mathbf{X}_{s,u} \otimes \Psi_{u,t} = \left(\sum_{|J| \leq N} b_J e_J \right) \otimes \Psi_{u,t} e_I = 1 \Psi_{u,t} (e_\emptyset \otimes e_I) + \left(\sum_{|J| > N} c_J e_J \right),$$

for some coefficients c_J , with $|J| > N$. We therefore have $\mathbf{X}_{s,u} \otimes_{\leq N} \Psi_{u,t} = \Psi_{u,t}$. The same reasoning applies to show that $\Psi_{s,u} \otimes_{\leq N} \mathbf{X}_{u,t} = \Psi_{s,u}$. For the last term in left-hand side of (3.6), let I be as above and $J = (0, \dots, 0, 1)$ with $|J| = N$. Then,

$$\Psi_{s,u} e_I \otimes \Psi_{u,t} e_J = \Psi_{s,u} \Psi_{u,t} e_I \otimes e_J.$$

As $e_I \otimes e_J \in V^{\otimes 2N}$, we have $\Psi_{s,u} \otimes_{\leq N} \Psi_{u,t} = 0$. Writing \otimes for $\otimes_{\leq N}$, it follows that

$$\mathbf{X}_{s,u} \otimes \Psi_{u,t} + \Psi_{s,u} \otimes \mathbf{X}_{u,t} + \Psi_{s,u} \otimes \Psi_{u,t} = \Psi_{s,u} + \Psi_{u,t} = \Psi_{s,t},$$

where the last equation follows from the additivity assumption. This completes the proof. \square

We now combine these results with the p -variation bounds on the functionals. Recall that a path $X : [0, T] \rightarrow V$ is α -Hölder continuous if, for $s \leq t \in [0, T]$ and $0 < \alpha \leq 1$,

$$|X_t - X_s| \leq C |t - s|^\alpha$$

for some constant $C > 0$. If X is α -Hölder continuous, then it has finite $1/\alpha$ -variation. The converse does not generally hold. However, if X is a continuous path with finite p -variation, there exists a continuous, increasing reparametrization τ such that $X \circ \tau$ is $1/p$ -Hölder continuous.

For a continuous functional $\mathbf{X} : \Delta_T \rightarrow T^N(V)$, we define

$$\|\mathbf{X}\|_{p\text{-var}} := \max_{1 \leq k \leq N} \sup_{\mathcal{D}} \left(\sum_{t_i \in \mathcal{D}} \|\pi_k(\mathbf{X}_{t_i, t_{i+1}})\|_{V^{\otimes k}}^{p/k} \right)^{k/p}, \quad (3.7)$$

where the sup is taken over all the partitions $\mathcal{D}_{[0, T]}$. If $\|\mathbf{X}\|_{p\text{-var}} < \infty$, the functional \mathbf{X} is said to have finite p -variation. The p -variation distance between two functionals \mathbf{X} and \mathbf{Y} of finite p -variation is defined as

$$d_{p\text{-var}}(\mathbf{X}, \mathbf{Y}) := \|\mathbf{X} - \mathbf{Y}\|_{p\text{-var}}. \quad (3.8)$$

Now assume that the multiplicative functionals $\mathbf{X}, \mathbf{Y} : \Delta_T \rightarrow T^N(V)$ have finite p -variation and agree on the first $N - 1$ levels. Then, as shown above, their difference at level N ,

$$\Psi_{s,t} = \mathbf{X}_{s,t}^N - \mathbf{Y}_{s,t}^N$$

defines an additive function on Δ_T . For a fixed $v \in V^{\otimes N}$, Ψ induces a path $\psi : [0, T] \rightarrow V^{\otimes N}$ by

$$\psi_t = v + \Psi_{0,t}.$$

Then, by additivity of Ψ ,

$$\Psi_{s,t} = \psi_t - \psi_s$$

for any $s \leq t$. Additivity implies that we can think of Ψ as a function that comes from the increments of a path.

As \mathbf{X} and \mathbf{Y} have finite p -variation, the difference Ψ at level N inherits finite p/N -variation. This follows directly from the structure of the p -variation norm (3.7), where the N -th level contributes with exponent p/N .

It follows that there exists a continuous and increasing reparametrization τ of $[0, T]$ such that the reparametrized path $\Psi \circ \tau$ (defined by $\Psi_{\tau(s), \tau(t)} = \psi_{\tau(t)} - \psi_{\tau(s)}$) is N/p -Hölder continuous. This means that ψ is regular enough to be treated as a genuine path in $V^{\otimes N}$, and that its increments

$\Psi_{s,t} = \psi_t - \psi_s$, are well-behaved. Regularity allows us to reinterpret Ψ as a “missing” top-level component that can be added to \mathbf{Y} to produce a new functional

$$\mathbf{Z}_{s,t} := \mathbf{Y}_{s,t} + \Psi_{s,t}.$$

By Lemma 3.16, \mathbf{Z} is indeed multiplicative (and of order N).

Now, suppose that $N/p > 1$. Then $\psi \circ \tau$ is Hölder continuous with exponent greater than 1, and thus must be constant. This implies that $\Psi_{s,t} = \psi_t - \psi_s = 0$ for all s, t , so the top level of \mathbf{X} and \mathbf{Y} must coincide:

$$\mathbf{X}^N = \mathbf{Y}^N.$$

Therefore, any two multiplicative functionals of finite p -variation that agree up to level $\lfloor p \rfloor$ must in fact agree entirely. This suggests that the levels up to $\lfloor p \rfloor$ determine the rest.

This observation raises the converse question: If a multiplicative functional \mathbf{X} is defined only up to level N , with finite p -variation and $N \geq \lfloor p \rfloor$, can we extend it to higher levels in a consistent way? That is, can we construct a full multiplicative functional $\mathbf{Y} : \Delta_T \rightarrow T^n(V)$ with $n > N$, such that \mathbf{Y} agrees with \mathbf{X} up to level N , and has finite p -variation?

Unlike the previous argument (no two extensions can differ when $N > \lfloor p \rfloor$), this one is about existence and uniqueness of such an extension. The following result, proved in Lyons et al. (2007), answers the question affirmatively.

Theorem 3.17 (Extension Theorem). *Let $p \geq 1$ be a real number, $N \geq 1$ an integer, and let $\mathbf{X} : \Delta_T \rightarrow T^N(V)$ be a multiplicative functional of degree N with finite p -variation. Suppose that $N \geq \lfloor p \rfloor$. Then, for every integer $n > N$, there exists a unique continuous multiplicative functional*

$$\mathbf{Y} : \Delta_T \rightarrow T^n(V)$$

such that

1. \mathbf{Y} agrees with \mathbf{X} up to level N ; that is, $\pi_{\leq N}(\mathbf{Y}) = \mathbf{X}$;
2. \mathbf{Y} has finite p -variation.

Moreover, the map that sends \mathbf{X} to its extension \mathbf{Y} is continuous with respect to the p -variation metric.

This result highlights that, for a multiplicative functional with finite p -variation, the first $\lfloor p \rfloor$ levels completely capture all of its information, leading naturally to the next definition.

Definition 3.18 (Rough Path). *Let $p \geq 1$. A p -rough path is a continuous multiplicative functional*

$$\mathbf{X} : \Delta_T \rightarrow T^{\lfloor p \rfloor}(V)$$

of degree $\lfloor p \rfloor$ with finite p -variation. The space of p -rough paths is denoted by $\Omega_T^p(V)$.

What distinguishes rough paths from general multiplicative functionals is that they retain only the minimal number of components necessary to capture all relevant information. In this sense, a rough path can be viewed as a “compressed” version of a multiplicative functional: it contains exactly the levels up to $\lfloor p \rfloor$, which fully determine the rest under finite p -variation.

So far, we have not explicitly relied on the theory of signatures of bounded variation paths, except to define objects that reflect some of their structural properties. Rough paths form a highly abstract class, while paths of bounded variation are concrete and familiar. It is therefore natural to examine the rough paths that are *close* to signatures of bounded variation paths, namely, those that arise as limits of such signatures. This leads us to the following definition.

Definition 3.19 (Geometric Rough Paths). *A geometric p -rough path is a p -rough path \mathbf{X} for which there exists a sequence of paths of bounded variation $\{X_n\}_{n \geq 1}$ such that*

$$\lim_{n \rightarrow \infty} d_{p\text{-var}}(\mathbf{X}, S(X_n)^{\leq \lfloor p \rfloor}) = 0.$$

The space of geometric p -rough paths is denoted by $G\Omega_T^p(V)$.

Recall from Proposition 3.12 that the signature of a bounded variation path satisfies the group-like property. It follows that each truncated signature $S(X_n)^{\leq [p]}$ takes values in $G^{[p]}(V)$, the set of group-like elements in the truncated tensor algebra $T^{[p]}(V)$.

Now, since the group-like property is algebraic and preserved under limits, and the geometric p -rough path \mathbf{X} is defined as the limit of such signatures in the p -variation topology, it also takes values in $G^{[p]}(V)$. Hence, every geometric p -rough path takes values in $G^{[p]}(V)$.

Note, however, that the converse does not hold in general: not every p -rough path taking values in $G^{[p]}(V)$ arises as the limit of signatures of bounded variation paths. This distinction motivates the following definition.

Definition 3.20 (Weakly Geometric Rough Paths). *A weakly geometric p -rough path is a p -rough path taking values in $G^{[p]}(V)$. The space of weakly geometric p -rough paths is denoted by $WG\Omega_T^p(V)$.*

The difference between $G\Omega_T^p(V)$ and $WG\Omega_T^p(V)$ is subtle and becomes relevant especially when V is infinite-dimensional. It is always the case that

$$G\Omega_T^p(V) \subset WG\Omega_T^p(V) \subset \Omega_T^p(V).$$

Example 3.21 (Brownian Motion). As we often work with Brownian motion in the context of signature-based models, it is worth pausing to examine its signature and its interpretation as a rough path.

Let $B : [0, T] \rightarrow \mathbb{R}^d$ be a standard d -dimensional Brownian motion, and assume that stochastic integrals with respect to B are defined in the Itô sense. Since Brownian motion has finite p -variation for any $p > 2$, we can attempt to lift it to a p -rough path with $p > 2$. The natural candidate for such a lift is the stochastic Itô signature:

$$\begin{aligned} S^{\text{Itô}}(B)_{s,t}^{\leq 2} &= \left(1, \int_s^t dB_u, \int_s^t \int_s^u dB_r dB_u \right) \\ &= \left(1, B_t - B_s, \int_s^t (B_u - B_s) dB_u \right) \\ &= \left(1, B_t - B_s, \frac{1}{2}(B_t - B_s)^2 - \frac{1}{2}(t - s) \right), \end{aligned}$$

where the last identity follows from Itô's isometry, using $B_t^2 - B_s^2 = 2 \int_s^t B_u dB_u + (t - s)$.

Now consider the shuffle identity. Since $e_1 \sqcup e_1 = 2e_1 \otimes e_1$, we have:

$$\langle e_1, S^{\text{Itô}}(B)_{s,t}^{\leq 2} \rangle^2 = (B_t - B_s)^2,$$

but

$$\langle e_1 \sqcup e_1, S^{\text{Itô}}(B)_{s,t}^{\leq 2} \rangle = 2 \cdot \left(\frac{1}{2}(B_t - B_s)^2 - \frac{1}{2}(t - s) \right) = (B_t - B_s)^2 - (t - s).$$

Therefore, as the multiplicative (Chen) identity fails, $S^{\text{Itô}}(B)_{s,t}^{\leq 2}$ is not group-like. It follows that the Itô signature does not define a weakly geometric rough path. Itô integration does not preserve algebraic structures compatible with rough path theory.

However, if we instead use Stratonovich integration, we obtain:

$$\begin{aligned} S^\circ(B)_{s,t}^{\leq 2} &= \left(1, \int_s^t \circ dB_u, \int_s^t \int_s^u \circ dB_r \circ dB_u \right) \\ &= \left(1, B_t - B_s, \frac{1}{2}(B_t - B_s)^2 \right). \end{aligned}$$

In this case

$$\langle e_1 \sqcup e_1, S^\circ(B)_{s,t}^{\leq 2} \rangle = 2 \cdot \frac{1}{2}(B_t - B_s)^2 = (B_t - B_s)^2$$

matches $\langle e_1, S^\circ(B)_{s,t}^{\leq 2} \rangle^2$, which means that the Stratonovich signature is group-like and defines a weakly geometric p -rough path for any $p > 2$.

Even though the Itô signature is not group-like, we are not at a dead end. There are at least two standard approaches. One is to construct a weakly geometric rough path lift of Brownian motion by defining the second level as the Stratonovich iterated integral, i.e., work with

$$\mathbf{B}_{s,t} := \left(1, B_t - B_s, \int_s^t (B_u - B_s) \circ dB_u \right),$$

which is group-like. This is known as the *Stratonovich lift* of Brownian motion and is the standard choice in rough path theory.

Alternatively, one could define a non-geometric rough path using the Itô integral, but the path would lie outside the standard tensor algebra and would need to incorporate Itô correction terms. This gives rise to *branched* or *generalized* rough paths (see Bruned et al. (2019)).

In general, the Stratonovich lift is preferred because it aligns with the algebraic structure of signatures (the group-like property) and allows for a direct interpretation of rough integrals as limits of classical Riemann–Stieltjes approximations. For one-dimensional paths, the following result shows that the situation is simpler.

Lemma 3.22. *Let $p \geq 1$ and let $X : [0, T] \rightarrow \mathbb{R}$ be a continuous path of finite p -variation. Then there exists a canonical lift to a weakly geometric p -rough path, given by*

$$\mathbf{X}_{s,t} = \left(1, X_t - X_s, \frac{(X_t - X_s)^2}{2!}, \dots, \frac{(X_t - X_s)^{\lfloor p \rfloor}}{\lfloor p \rfloor!} \right).$$

This expression defines a valid lift because, in the one-dimensional case (see Example 3.8), all iterated integrals reduce to powers of the increment. More precisely, the right-hand side of the equation is the truncated exponential in the tensor algebra

$$\exp_{\otimes}^{\leq \lfloor p \rfloor}(X_t - X_s) = \left(1, X_t - X_s, \frac{(X_t - X_s)^2}{2!}, \dots, \frac{(X_t - X_s)^{\lfloor p \rfloor}}{\lfloor p \rfloor!} \right),$$

which is known to satisfy the Chen identity. (We use the notation \exp_{\otimes} to indicate that the exponential is taken in the tensor algebra.)

Since X has finite p -variation and each level k is a smooth function of the increment $X_t - X_s$, the k -th level has finite p/k -variation. Hence, the full lift \mathbf{X} has finite p -variation in the sense of (3.7), and defines a weakly geometric p -rough path.

In particular, for a one-dimensional Brownian motion $B : [0, T] \rightarrow \mathbb{R}$, the path

$$\mathbf{B}_{s,t} := \left(1, B_t - B_s, \frac{1}{2}(B_t - B_s)^2 \right)$$

defines a weakly geometric p -rough path for any $p > 2$. This *Stratonovich lift* of Brownian motion corresponds to the first two levels of the Stratonovich signature.

3.4 Time-Augmented Rough Paths

Recall that a *lifted* path refers to extending a base path $X : [0, T] \rightarrow V$ to a rough path $\mathbf{X} : \Delta_T \rightarrow T^N(V)$. We now proceed to *augment* X with a time coordinate. Specifically, we define $\hat{X} : [0, T] \rightarrow \mathbb{R} \oplus V$ by

$$\hat{X}_t := (t, X_t).$$

At first glance, this change may appear superficial, but it has important consequences that we discuss at the end of this section.

The following important proposition says that time augmentation preserves important analytic and algebraic properties, such as admitting a lift to a weakly geometric p -rough path.

Proposition 3.23. *Let $X : [0, T] \rightarrow V$ be a continuous path that admits a weakly geometric p -rough path lift $\mathbf{X} \in W\Omega_T^p(V)$. Define the time-augmented path $\hat{X} : [0, T] \rightarrow \mathbb{R} \oplus V$ by*

$$\hat{X}_t := (t, X_t).$$

Then \hat{X} also admits a weakly geometric p -rough path lift $\hat{\mathbf{X}} \in W\Omega_T^p(\mathbb{R} \oplus V)$.

Proof. We treat \hat{X} as a path in \mathbb{R}^{d+1} , where the first coordinate is time and the remaining ones are given by X . We define the lifted path $\hat{\mathbf{X}}$ inductively over multi-indices $I = (i_1, \dots, i_n) \in \{0, 1, \dots, d\}^n$, where $i_k = 0$ refers to the time component.

For $|I| = 1$, we set:

$$\hat{\mathbf{X}}_{s,t}^i = \begin{cases} t - s & \text{if } i = 0, \\ X_t^i - X_s^i & \text{if } i \in \{1, \dots, d\}. \end{cases}$$

For higher levels, we proceed inductively. If all $i_k \neq 0$, we set $\hat{\mathbf{X}}_{s,t}^I := \mathbf{X}_{s,t}^I$, which is already defined in the original lift.

If the multi-index I includes at least one zero, say $i_k = 0$, we define $\hat{\mathbf{X}}_{s,t}^I$ via recursive integration, using the property:

$$\hat{\mathbf{X}}_{s,t}^I := \int_s^t \hat{\mathbf{X}}_{s,u}^{\dot{I}} du,$$

where \dot{I} is the multi-index I with the zero component i_k removed. We give an example of the inductive step. Assume that $\hat{\mathbf{X}}$ has been defined up to level $n-1$. The n -th level components are $\langle e_I, \hat{\mathbf{X}}_{s,t} \rangle$, where $I = (i_1, \dots, i_n)$. Assume $i_k = 0$ for some k . By the definition of the shuffle product,

$$e_I = e_{I'} \sqcup e_{i_n} - (e_{I''} \sqcup e_{i_n}) \otimes e_{i_{n-1}},$$

where I' has the same meaning as in Definition 3.3. We then have

$$\begin{aligned} \langle e_I, \hat{\mathbf{X}}_{s,t} \rangle &= \langle e_{I'} \sqcup e_{i_n} - (e_{I''} \sqcup e_{i_n}) \otimes e_{i_{n-1}}, \hat{\mathbf{X}}_{s,t} \rangle \\ &= \langle e_{I'} \sqcup e_{i_n}, \hat{\mathbf{X}}_{s,t} \rangle - \langle (e_{I''} \sqcup e_{i_n}) \otimes e_{i_{n-1}}, \hat{\mathbf{X}}_{s,t} \rangle. \end{aligned}$$

Note that the first term on the right-hand side satisfies the group-like property because of the induction step ($|I'| = n-1$ and $|i_n| = 1$), so we can therefore write

$$\langle e_I, \hat{\mathbf{X}}_{s,t} \rangle = \langle e_{I'}, \hat{\mathbf{X}}_{s,t} \rangle \langle e_{i_n}, \hat{\mathbf{X}}_{s,t} \rangle - \langle (e_{I''} \sqcup e_{i_n}) \otimes e_{i_{n-1}}, \hat{\mathbf{X}}_{s,t} \rangle.$$

For the second term, we consider two cases. If $i_{n-1} = 0$, we define

$$\begin{aligned} \langle (e_{I''} \sqcup e_{i_n}) \otimes e_{i_{n-1}}, \hat{\mathbf{X}}_{s,t} \rangle &= \int_s^t \langle e_{I''} \sqcup e_{i_n}, \hat{\mathbf{X}}_{s,u} \rangle d\hat{X}_u^{i_{n-1}} \\ &:= \int_s^t \langle e_{I''} \sqcup e_{i_n}, \hat{\mathbf{X}}_{s,u} \rangle du. \end{aligned}$$

If $i_{n-1} \neq 0$, we repeat the process until we reach the i_k that is equal to zero. This procedure is well-defined because integration with respect to time is always available, and the shuffle relations ensure compatibility with Chen's identity. The inductive definition guarantees that the resulting path $\hat{\mathbf{X}}$ is multiplicative and has finite p -variation. Therefore, $\hat{\mathbf{X}} \in W\Omega_T^p(\mathbb{R} \oplus V)$ defines a valid weakly geometric p -rough path lift of \hat{X} . \square

Now that we know that there exists a lift for the time-augmented path \hat{X} , we define the corresponding space.

Definition 3.24 (Time-Augmented Weakly Geometric Rough Path). *A time-augmented weakly geometric p -rough path is a weakly geometric p -rough path $\mathbf{X} \in W\Omega_T^p(\mathbb{R} \oplus V)$ such that the first level satisfies*

$$\pi_1(\mathbf{X}_{s,t}) = \hat{X}_t - \hat{X}_s,$$

where $\hat{X}_t = (t, X_t)$, for some continuous path $X : [0, T] \rightarrow V$ that admits a weakly geometric p -rough path lift. We denote the space of such paths by $W\hat{\Omega}_T^p(V)$.

Remark 3.25. A rough path in $WG\hat{\Omega}_T^p(V)$ presupposes the existence of a base path $X : [0, T] \rightarrow V$, which is augmented to $\hat{X} : [0, T] \rightarrow \mathbb{R} \oplus V$. This contrasts with the rough paths in $WG\Omega_T^p(V)$, which are defined independently of any base path.

We now briefly discuss the relevance of lifting the augmented path (t, X_t) instead of lifting X_t alone. Let $S(X)$ denote the signature of a path $X : [0, T] \rightarrow V$. It is well known that the map $X \mapsto S(X)$ is not injective: different paths can share the same signature—for example, if they trace out the same image at different speeds. Thus, the signature loses information about the timing or parametrization of the path.

Augmenting the path by adding time, that is, lifting $\hat{X}_t := (t, X_t) \in \mathbb{R} \oplus V$, recovers injectivity up to reparametrization. As we will see in Theorem 3.27, the time-augmented signature uniquely determines the path, making it more expressive.

Time augmentation allows the signature to distinguish between paths that follow the same geometric shape but evolve at different speeds. This distinction is crucial in the context of the universal approximation theorems discussed below: time augmentation ensures that the signature map separates paths in a sufficiently rich way to apply approximation results such as the Stone–Weierstrass theorem.

As we will also see below, time augmentation is essential for learning path-dependent functionals in an *adapted* way. In models where Y_t depends on the past trajectory $(X_s)_{s \leq t}$, incorporating time allows the signature to detect when events occur. Without time, the signature treats two paths with the same shape but different timing as indistinguishable—an undesirable feature in many stochastic or temporally sensitive learning tasks.

3.5 Signatures of Rough Paths

Let $\mathbf{X} \in \Omega_T^p(V)$ be a p -rough path. By the extension theorem, for every integer $N \geq \lfloor p \rfloor$, there exists a unique multiplicative extension of \mathbf{X} to degree N with finite p -variation. Since this extension process can be carried out to arbitrarily high degrees, it is natural to define the *signature* of a p -rough path as its formal infinite extension. This motivates the following definition.

Definition 3.26 (Signature of a Rough Path). *Let $\mathbf{X} \in \Omega_T^p(V)$ be a p -rough path. The truncated signature of order $N \geq \lfloor p \rfloor$ is defined as the unique extension of \mathbf{X} to level N , denoted by:*

$$S(\mathbf{X})^{\leq N} := (1, S(\mathbf{X})^1, \dots, S(\mathbf{X})^N) \in T^N(V).$$

The (full) signature of \mathbf{X} is the formal series

$$\begin{aligned} S(\mathbf{X}) : \Delta_T &\rightarrow T((V)) \\ (s, t) &\mapsto S(\mathbf{X})_{s,t} := (1, S(\mathbf{X})_{s,t}^1, \dots, S(\mathbf{X})_{s,t}^n, \dots), \end{aligned}$$

where $S(\mathbf{X})_{s,t}^n \in V^{\otimes n}$ denotes the n -th level of the extension.

Let $\mathbf{X} \in WG\Omega_T^p(V)$ and $1 < p < q$. In Friz and Victoir (2010) it is proved that

$$WG\Omega_T^p(V) \subset G\Omega_T^q(V).$$

Therefore, there exists a sequence of bounded variation paths $X^{(n)}$ such that their truncated signatures of order $\lfloor q \rfloor$ converge to \mathbf{X} in the q -variation topology. By Theorem 3.17, the extension map $\mathbf{X} \mapsto S(\mathbf{X})^{\leq \lfloor q \rfloor}$ is continuous in the q -variation topology. Since each $S(X^{(n)})^{\leq \lfloor q \rfloor}$ is group-like, it follows that $S(\mathbf{X})^{\leq \lfloor q \rfloor}$ is group-like as well. Letting $q \rightarrow \infty$, we obtain that the full signature $S(\mathbf{X}) \in T((V))$ is group-like. That is, for any $\ell^1, \ell^2 \in T(V)$, we have:

$$\langle \ell^1, S(\mathbf{X})_{s,t} \rangle \langle \ell^2, S(\mathbf{X})_{s,t} \rangle = \langle \ell^1 \sqcup \ell^2, S(\mathbf{X})_{s,t} \rangle.$$

Note the slight shift in notation that has taken place here. In Section 3.2, we began with a path $X : [0, T] \rightarrow V$ and constructed its signature, denoted by $S(X) : \Delta_T \rightarrow T((V))$. In contrast, we

now start with a multiplicative functional $\mathbf{X} : \Delta_T \rightarrow T^{[p]}(V)$, which satisfies specific algebraic and analytic properties (multiplicativity and finite p -variation) that allow it to be uniquely extended to all higher levels $N \geq [p]$. We can describe this extension process using the diagram:

$$\begin{array}{ccccc} \mathbf{X}^{[p]}(V) & \longrightarrow & \mathbf{X}^N(V) & \longrightarrow & \mathbf{X}^\infty \\ (1, \mathbf{X}_{s,t}^1, \dots, \mathbf{X}_{s,t}^{[p]}) & \longrightarrow & (1, \mathbf{X}_{s,t}^1, \dots, \mathbf{X}_{s,t}^N) & \longrightarrow & (1, \mathbf{X}_{s,t}^1, \dots, \mathbf{X}_{s,t}^n, \dots) \end{array}$$

where we slightly abuse notation in referring to \mathbf{X}^∞ as the infinite extension of the rough path.

In Definition 3.26, however, we formalized this extension using the signature notation:

$$\begin{array}{ccccc} \mathbf{X}^{[p]}(V) & \longrightarrow & S(\mathbf{X})^{\leq N}(V) & \longrightarrow & S(\mathbf{X}) \\ (1, \mathbf{X}_{s,t}^1, \dots, \mathbf{X}_{s,t}^{[p]}) & \longrightarrow & (1, S(\mathbf{X})_{s,t}^1, \dots, S(\mathbf{X})_{s,t}^N) & \longrightarrow & (1, S(\mathbf{X})_{s,t}^1, \dots, S(\mathbf{X})_{s,t}^n, \dots) \end{array}$$

Note carefully that we have not *constructed a signature* from \mathbf{X} . Rather, we started with a multiplicative functional satisfying the group-like property and finite p -variation, and considered its projection to the first $[p]$ levels to define a rough path. By Theorem 3.17, this functional can be uniquely extended to higher levels in the (truncated) tensor algebra. In Definition 3.26, we have simply relabeled this extended functional using the signature notation previously introduced for bounded variation paths.

Although this notation may initially appear inconsistent, it aligns naturally with the classical case where the signature is defined via iterated integrals. This unification of notation allows both settings—bounded variation and rough paths—to be treated within a common framework.

3.6 Universal Approximation Theorems

Since the primary role of a rough path \mathbf{X} is to serve as a driver for integrals (or differential equations), the key object of interest is the increment $\mathbf{X}_{s,t}$ rather than the individual value \mathbf{X}_t at a fixed time. But the two viewpoints are equivalent. Given the increments $\mathbf{X}_{s,t}$, one can reconstruct a path by defining $\mathbf{X}_t := \mathbf{X}_{0,t}$. If the path $\mathbf{X}_t \in T^N(V)$ is given, the increments can be recovered by making use of the multiplicative property, namely, $\mathbf{X}_{s,t} := \mathbf{X}_s^{-1} \otimes \mathbf{X}_t$.

In this section, we present three fundamental theorems that enable the application of signatures to the calibration problem. The first addresses the uniqueness of the signature: it states that the signature (as defined in Definition 3.26) of a time-augmented weakly geometric p -rough path \mathbf{X} , evaluated at time T , uniquely determines \mathbf{X} . We use the simplified notation $\mathbf{X}_t := \mathbf{X}_{0,t}$.

Theorem 3.27 (Uniqueness of the Signature). *Let $\mathbf{X}, \mathbf{Y} \in WG\hat{\Omega}_T^p(V)$. Then,*

$$S(\mathbf{X})_T = S(\mathbf{Y})_T \iff \forall t \in [0, T], \mathbf{X}_t = \mathbf{Y}_t.$$

Proof. Note first that $\mathbf{X} : \Delta_T \rightarrow T^{[p]}(\mathbb{R} \oplus V)$, while $S(\mathbf{X}) : \Delta_T \rightarrow T((\mathbb{R} \oplus V))$. If $\mathbf{X}_t = \mathbf{Y}_t$ for all $t \in [0, T]$, it must be that $\mathbf{X}_T = \mathbf{Y}_T$. By the extension theorem, $S(\mathbf{X})_T = S(\mathbf{Y})_T$.

Reciprocally, assume $S(\mathbf{X})_T = S(\mathbf{Y})_T$. Since $\mathbf{X}, \mathbf{Y} \in WG\hat{\Omega}_T^p(V)$ and both coincide with their signatures up to level $[p]$, it suffices to show that for any multi-index I with $|I| \leq [p]$,

$$\langle e_I, \mathbf{X}_t \rangle = \langle e_I, \mathbf{Y}_t \rangle \quad \text{for all } t \in [0, T].$$

To extract these values from the full signature $S(\mathbf{X})_T$, we face the difficulty that $\langle e_I, \mathbf{X}_t \rangle$ is a function of time, not a coefficient in the signature at time T . However, we can recover such functions by integrating them against powers of time. To do this, we first prove that:

$$\langle e_0^{\otimes k}, \mathbf{X}_t \rangle = \frac{t^k}{k!} \quad \text{for all } k \geq 0.$$

We proceed by induction. For $k = 0$, the claim is trivial. For $k = 1$, we have $\langle e_0, \mathbf{X}_t \rangle = t$ by the definition of time augmentation. Assuming the identity holds for $k - 1$, we get:

$$\langle e_0^{\otimes k}, \mathbf{X}_t \rangle = \int_0^t \langle e_0^{\otimes(k-1)}, \mathbf{X}_u \rangle du = \int_0^t \frac{u^{k-1}}{(k-1)!} du = \frac{t^k}{k!}.$$

Now fix any multi-index I with $|I| \leq [p]$. Since \mathbf{X}_t and $S(\mathbf{X})_t$ agree up to level $[p]$, we have

$$\langle e_I, S(\mathbf{X})_t \rangle = \langle e_I, \mathbf{X}_t \rangle.$$

Using the group-like property and the shuffle product identity, for $k \leq [p]$ we obtain:

$$\begin{aligned} \langle (e_I \sqcup e_0^{\otimes k}) \otimes e_0, S(\mathbf{X})_T \rangle &= \int_0^T \langle e_I \sqcup e_0^{\otimes k}, S(\mathbf{X})_u \rangle du \\ &= \int_0^T \langle e_I, S(\mathbf{X})_u \rangle \langle e_0^{\otimes k}, S(\mathbf{X})_u \rangle du \\ &= \int_0^T \langle e_I, \mathbf{X}_u \rangle \frac{u^k}{k!} du. \end{aligned}$$

Applying the same reasoning to \mathbf{Y} , and using the assumption $S(\mathbf{X})_T = S(\mathbf{Y})_T$, we conclude that:

$$\int_0^T (\langle e_I, \mathbf{X}_u \rangle - \langle e_I, \mathbf{Y}_u \rangle) \frac{u^k}{k!} du = 0 \quad \text{for all } k \geq 0.$$

Since the functions $u \mapsto \frac{u^k}{k!}$ (for $k \geq 0$) form a basis for the space of polynomials, and polynomials are dense in $C([0, T])$ by the Stone–Weierstrass theorem, it follows that any continuous function whose integral against every such monomial vanishes must itself be identically zero. As \mathbf{X}_u and \mathbf{Y}_u are continuous, it follows that

$$\langle e_I, \mathbf{X}_u \rangle = \langle e_I, \mathbf{Y}_u \rangle \quad \text{for all } u \in [0, T],$$

which completes the proof. \square

Before proceeding, note that $WG\hat{\Omega}_T^p(V)$, equipped with the p -variation distance, becomes a topological space whose topology is induced by the p -variation metric.

Theorem 3.28 (First Universal Approximation Theorem). *Let $K \subset WG\hat{\Omega}_T^p(V)$ be compact, and let $f : WG\hat{\Omega}_T^p(V) \rightarrow \mathbb{R}$ be continuous with respect to the p -variation topology. Then, for every $\varepsilon > 0$, there exists $\ell \in T(\mathbb{R} \oplus V)$ such that*

$$\sup_{\mathbf{X} \in K} |f(\mathbf{X}) - \langle \ell, S(\mathbf{X})_T \rangle| < \varepsilon.$$

Proof. We apply the Stone–Weierstrass theorem to a suitable subalgebra of continuous functions on the compact set $K \subset WG\hat{\Omega}_T^p(V)$. Define

$$A := \text{span} \{ \mathbf{X} \mapsto \langle e_I, S(\mathbf{X})_T \rangle; I \text{ multi-index in } \mathbb{R} \oplus V \} \subset C(K).$$

That is, A is the collection of all finite linear combinations of coordinate functionals on the signature evaluated at time T .

To show that A is a subalgebra of $C(K)$ that satisfies the conditions of the Stone–Weierstrass theorem, consider first that A is closed under multiplication: as the group-like property

$$\langle \ell_1 \sqcup \ell_2, S(\mathbf{X})_T \rangle = \langle \ell_1, S(\mathbf{X})_T \rangle \langle \ell_2, S(\mathbf{X})_T \rangle$$

corresponds to multiplication of linear functionals on the signature, the span of such functionals is closed under multiplication. Second, A separates points in K due to the uniqueness of the signature of time-augmented weakly geometric rough paths: in particular, Theorem 3.27 guarantees that

if $\mathbf{X} \neq \mathbf{Y}$ in K , then $S(\mathbf{X})_T \neq S(\mathbf{Y})_T$, so there exists $\ell \in T(\mathbb{R} \oplus V)$ such that $\langle \ell, S(\mathbf{X})_T \rangle \neq \langle \ell, S(\mathbf{Y})_T \rangle$. And third, A contains the constant functions, as can be seen by choosing $I = \emptyset$, for which $\langle e_I, S(\mathbf{X})_T \rangle = 1$.

Therefore, by the Stone–Weierstrass theorem, A is dense in $C(K)$. In particular, for any $\varepsilon > 0$, there exists $\ell \in T(\mathbb{R} \oplus V)$ such that

$$\sup_{\mathbf{X} \in K} |f(\mathbf{X}) - \langle \ell, S(\mathbf{X})_T \rangle| < \varepsilon.$$

□

This result is important. The signature $S(\mathbf{X})$, evaluated at time T , serves as a feature map that transforms a path into an infinite sequence of coordinates capturing all relevant information. Theorem 3.27 ensures that this representation is injective for time-augmented paths. It is then natural to ask whether signatures are rich enough to approximate functionals defined on paths. The First Universal Approximation Theorem answers this question affirmatively.

It specifically states that continuous functionals on compact subsets of the rough path space can be approximated arbitrarily well by linear functionals on the signature—that is, by finite linear combinations of iterated integrals. This makes signatures a powerful tool for representing and learning functionals on paths, especially in contexts such as calibration or supervised learning.

Our goal is to model one-dimensional stochastic processes of the form

$$Y_t = f((\mathbf{X}_s)_{s \in [0, t]}),$$

where $\mathbf{X} = (\mathbf{X}_t)_{t \in [0, T]}$ is a stochastic process taking values in the space of time-augmented weakly geometric p -rough paths; that is, each $\mathbf{X}_t \in WG\hat{\Omega}_t^p(V)$. Think of Y_t as a volatility process driven by a rough signal \mathbf{X} . The function f , which encodes this dependence, is typically unknown.

A technical issue arises because, as time increases, the domain of f changes: for each t , the input $(\mathbf{X}_s)_{s \in [0, t]}$ represents a collection of rough paths defined on a different time interval. To deal with this, we need a consistent way to interpret a rough path in $WG\hat{\Omega}_s^p(V)$ as an element of $WG\hat{\Omega}_t^p(V)$ for all $t \geq s$, so that f can act on a common space.

The idea is to extend \mathbf{X} from $[0, s]$ to $[0, t]$ by keeping it constant after time s . Since we work with time-augmented rough paths, it does not make sense to freeze the time component; therefore, only the spatial component will be "stopped." We now make this construction precise.

Given the potential complexity of the notation, we begin with a simple case and build up from there. Let $\mathbf{X} \in WG\hat{\Omega}_T^p(V)$ be represented by the diagram:

$$\begin{aligned} \Delta_T &\longrightarrow T^{[p]}(\mathbb{R} \oplus V) \\ (s, t) &\longmapsto \mathbf{X}_{s, t} = \left(1, \mathbf{X}_{s, t}^1, \dots, \mathbf{X}_{s, t}^{[p]}\right), \end{aligned}$$

for $0 \leq s \leq t \leq T$. Fixing $s = 0$, we write $\mathbf{X}_t := \mathbf{X}_{0, t}$.

Now consider a rough path $\mathbf{X} \in WG\hat{\Omega}_s^p(V)$ defined over $[0, s]$. For $r \leq u \leq s$, we write:

$$\begin{aligned} \Delta_s &\longrightarrow T^{[p]}(\mathbb{R} \oplus V) \\ (r, u) &\longmapsto \mathbf{X}_{r, u}^{[s]} = \left(1, \mathbf{X}_{r, u}^{[s]1}, \dots, \mathbf{X}_{r, u}^{[s][p]}\right), \end{aligned}$$

where we denote the path by $\mathbf{X}^{[s]}$ to emphasize that it lives on $[0, s]$. For $u \in [0, s]$, we write $\mathbf{X}_u^{[s]} := \mathbf{X}_{0, u}^{[s]}$.

By Proposition 3.23, a rough path in $WG\hat{\Omega}_s^p(V)$ originates from a base path $X : [0, s] \rightarrow V$ that admits a lift $\mathcal{X}^{[s]} \in WG\Omega_s^p(V)$. The corresponding diagram is:

$$\begin{aligned} \Delta_s &\longrightarrow T^{[p]}(V) \\ (r, u) &\longmapsto \mathcal{X}_{r, u}^{[s]} = \left(1, \mathcal{X}_{r, u}^{[s]1}, \dots, \mathcal{X}_{r, u}^{[s][p]}\right). \end{aligned}$$

For $u \in [0, s]$, we write $\mathcal{X}_u^{[s]} := \mathcal{X}_{0,u}^{[s]}$.

We now define the time-augmented path $\hat{X}_u := (u, X_u)$ for $u \in [0, s]$. Again by Proposition 3.23, \hat{X} admits a weakly geometric p -rough path lift $\hat{\mathcal{X}}^{[s]} \in WG\hat{\Omega}_s^p(V)$.

To extend this to the interval $[0, t]$, we first define the spatial component $\mathcal{X}^{[t]} \in WG\Omega_t^p(V)$ by:

$$\mathcal{X}_u^{[t]} := \begin{cases} \mathcal{X}_u^{[s]} & \text{for } u \in [0, s], \\ \mathcal{X}_s^{[s]} & \text{for } u \in [s, t], \end{cases}$$

that is, the spatial path is frozen after time s . We then apply the construction from the proof of Proposition 3.23 to obtain a time-augmented rough path $\hat{\mathcal{X}}^{[t]} \in WG\hat{\Omega}_t^p(V) \subset WG\Omega_t^p(\mathbb{R} \oplus V)$. By construction, $\hat{\mathcal{X}}^{[t]}$ agrees with $\hat{\mathcal{X}}^{[s]}$ on $[0, s]$.

This provides a consistent way to extend truncated rough paths defined on $[0, s]$ to the full interval $[0, t]$, thus allowing the functional f to act on a unified space. The ability to extend time-augmented paths motivates the following definition.

Definition 3.29 (Stopped Rough Path). *Let $p \geq 1$. We define the space of weakly geometric stopped p -rough paths as*

$$\Lambda_T^p(V) := \bigcup_{t \in [0, T]} WG\hat{\Omega}_t^p(V).$$

Given $\mathbf{X}^{[s]} \in WG\hat{\Omega}_s^p(V)$ and $\mathbf{Y}^{[t]} \in WG\hat{\Omega}_t^p(V)$, with $s \leq t$, we define a metric on $\Lambda_T^p(V)$ by

$$d(\mathbf{X}^{[s]}, \mathbf{Y}^{[t]}) := d_{p\text{-var}}^{[t]}(\hat{\mathbf{X}}^{[t]}, \mathbf{Y}^{[t]}) + |t - s|,$$

where $\hat{\mathbf{X}}^{[t]}$ denotes the extension of $\mathbf{X}^{[s]}$ from $[0, s]$ to $[0, t]$ as described above, and $d_{p\text{-var}}^{[t]}$ denotes the p -variation distance on $WG\hat{\Omega}_t^p(V)$.

For further details on the topology of this space, see Kalsi et al. (2020) and Bayer et al. (2023). The concept of stopped rough paths provides a useful framework for handling adaptedness in stochastic settings. The Second Universal Approximation Theorem below is formulated in this space.

Theorem 3.30 (Second Universal Approximation Theorem). *Let $K \subset WG\hat{\Omega}_T^p(V)$ be a compact subset, and let $f : \Lambda_T^p(V) \rightarrow \mathbb{R}$ be a continuous function. Then, for every $\varepsilon > 0$, there exists $\ell \in T(\mathbb{R} \oplus V)$ such that*

$$\sup_{\mathbf{X} \in K, t \in [0, T]} \left| f(\mathbf{X}^{[t]}) - \langle \ell, S(\mathbf{X}^{[t]})_t \rangle \right| < \varepsilon,$$

where $\mathbf{X}^{[t]}$ denotes the restriction of \mathbf{X} to $[0, t]$, and $S(\mathbf{X}^{[t]})_t := S(\mathbf{X}^{[t]})_{0,t}$ is the signature of the stopped rough path up to time t .

Proof. The proof follows the same lines as the first universal approximation theorem. \square

This result shows that any continuous functional of a stopped rough path can be uniformly approximated, over all truncating times $t \in [0, T]$ and all paths in a compact set, by a linear functional on the signature. The approximation is uniform both in path space and in time.

4 Signature-Based Volatility Models

Assume $r = 0$, and let $\{S_t; t \in [0, T]\}$ denote the price process of a risky asset. We work under a risk-neutral measure, and model the discounted stock price $\tilde{S}_t := S_t$ as

$$d\tilde{S}_t = \tilde{S}_t \sigma_t dB_t,$$

where σ_t is the market volatility and B is a standard Brownian motion.

Let $f : \Lambda_T^p(V) \rightarrow \mathbb{R}$ be a continuous function and suppose that volatility can be expressed as

$$\sigma_t = f((\mathbf{X}_s)_{s \in [0, t]}),$$

where the stochastic process $\mathbf{X} \in \Lambda_T^p(V)$ is referred to as the *primary process*. This process represents the underlying source of noise driving the volatility and is assumed to take values in the space of stopped, time-augmented weakly geometric p -rough paths.

Fix an integer $N \geq 1$, and define the space

$$A_N := \text{span} \{ \mathbf{X} \mapsto \langle e_I, S(\mathbf{X})_T \rangle \mid I \text{ multi-index in } \mathbb{R} \oplus V, 0 \leq |I| \leq N \},$$

where $S(\mathbf{X})_t := S(\mathbf{X}^{[t]})_{0,t}$ denotes the signature of the stopped path $\mathbf{X}^{[t]}$.

Our goal is to find, for a given $N \geq 1$, the coefficients $\ell = \{\ell_I; 0 \leq |I| \leq N\}$ that yield the best linear approximation

$$\langle \ell, S(\mathbf{X})_t^{\leq N} \rangle = \sum_{|I| \leq N} \ell_I \langle e_I, S(\mathbf{X})_t^{\leq N} \rangle$$

of the volatility σ_t , where $S(\mathbf{X})_t^{\leq N} \in T^N(\mathbb{R} \oplus V)$. This leads to the following signature-based stochastic volatility model:

$$\begin{aligned} d\tilde{S}_t(\ell) &= \tilde{S}_t(\ell) \sigma_t(\ell) dB_t, \\ \sigma_t(\ell) &= \sum_{|I| \leq N} \ell_I \langle e_I, S(\mathbf{X})_t^{\leq N} \rangle. \end{aligned} \tag{4.1}$$

Note that since \mathbf{X} is a stochastic process, the signature $S(\mathbf{X})_t^{\leq N}$ is itself a stochastic process taking values in the truncated tensor algebra $T^N(\mathbb{R} \oplus V)$.

Example 4.1. Assume the volatility dynamics follows the Heston model:

$$\begin{aligned} dS_t &= rS_t dt + X_t S_t d(\rho W_t + \sqrt{1 - \rho^2} B_t), \\ dX_t &= \kappa(\theta - X_t) dt + \nu \sqrt{X_t} dW_t, \end{aligned} \tag{4.2}$$

where $\kappa, \theta, \nu > 0$, and W and B are independent standard Brownian motions. We assume that X_t admits a time-augmented weakly geometric p -rough path lift $\mathbf{X} \in WG\hat{\Omega}_T^p(\mathbb{R} \oplus \mathbb{R})$, where the time component corresponds to coordinate 0 and the volatility component to coordinate 1.

Let $f : \Lambda_T^p(\mathbb{R}) \rightarrow \mathbb{R}$ be an unknown continuous function. We model the volatility as

$$\sigma_t = f((\mathbf{X}_s)_{s \leq t}),$$

and approximate it using the truncated signature up to level $N = 2$:

$$\sigma_t(\ell) = \sum_{|I| \leq 2} \ell_I \langle e_I, S(\mathbf{X})_t^{\leq 2} \rangle,$$

where $S(\mathbf{X})_t = S(\mathbf{X}^{[t]})_{0,t}$ is the signature of the stopped path \mathbf{X} up to time t . For $N = 2$, the truncated signature has the form:

$$S(\mathbf{X})_t^{\leq 2} = \left(1, (t, X_t), \begin{pmatrix} \int_0^t s ds & \int_0^t s dX_s \\ \int_0^t X_s ds & \int_0^t X_s dX_s \end{pmatrix} \right).$$

If we now consider

$$\ell = (\ell_\emptyset, \ell_0, \ell_1, \ell_{00}, \ell_{01}, \ell_{10}, \ell_{11}),$$

we have the following linear model for volatility:

$$\sigma_t(\ell) = \ell_\emptyset + \ell_0 t + \ell_1 X_t + \ell_{00} t^2 + \ell_{01} \int_0^t s dX_s + \ell_{10} \int_0^t X_s ds + \ell_{11} \int_0^t X_s dX_s.$$

Differentiating $\sigma_t(\ell)$ with respect to t and substituting the dynamics of X_t as in (4.2) yields:

$$\begin{aligned} d\sigma_t(\ell) &= (\ell_0 + \ell_{00}t + \ell_{10}X_t + (\ell_1 + \ell_{01}t + \ell_{11}X_t) \kappa(\theta - X_t)) dt \\ &\quad + \nu\sqrt{X_t} (\ell_1 + \ell_{01}t + \ell_{11}X_t) dW_t. \end{aligned}$$

This expression shows how a linear signature model recovers a volatility process consistent with the Heston dynamics.

Continuing with the example, the third level of the time-augmented signature, $S(\mathbf{X})_t^3$, consists of iterated integrals over $0 < u_1 < u_2 < u_3 < t$, indexed by $I = (i_1, i_2, i_3) \in \{0, 1\}^3$. A few representative terms are:

$$\begin{aligned} \langle e_{000}, S(\mathbf{X})_t \rangle &= \int_0^t \int_0^{u_2} \int_0^{u_1} du_0 du_1 du_2 = \frac{t^3}{6}, \\ \langle e_{001}, S(\mathbf{X})_t \rangle &= \int_0^t \int_0^{u_2} \int_0^{u_1} du_0 du_1 dX_{u_2}, \\ \langle e_{011}, S(\mathbf{X})_t \rangle &= \int_0^t \int_0^{u_2} \int_0^{u_1} du_0 dX_{u_1} dX_{u_2}, \\ \langle e_{111}, S(\mathbf{X})_t \rangle &= \int_0^t \int_0^{u_2} \int_0^{u_1} dX_{u_0} dX_{u_1} dX_{u_2}. \end{aligned}$$

In total, the third level of the time-augmented signature includes $2^3 = 8$ terms:

$$\begin{pmatrix} \langle e_{000}, S(\mathbf{X})_t \rangle & \langle e_{001}, S(\mathbf{X})_t \rangle \\ \langle e_{010}, S(\mathbf{X})_t \rangle & \langle e_{011}, S(\mathbf{X})_t \rangle \\ \langle e_{100}, S(\mathbf{X})_t \rangle & \langle e_{101}, S(\mathbf{X})_t \rangle \\ \langle e_{110}, S(\mathbf{X})_t \rangle & \langle e_{111}, S(\mathbf{X})_t \rangle \end{pmatrix} = \begin{pmatrix} \int_0^t \int_0^{u_2} \int_0^{u_1} du_0 du_1 du_2 & \int_0^t \int_0^{u_2} \int_0^{u_1} du_0 du_1 dX_{u_2} \\ \int_0^t \int_0^{u_2} \int_0^{u_1} du_0 dX_{u_1} du_2 & \int_0^t \int_0^{u_2} \int_0^{u_1} du_0 dX_{u_1} dX_{u_2} \\ \int_0^t \int_0^{u_2} \int_0^{u_1} dX_{u_0} du_1 du_2 & \int_0^t \int_0^{u_2} \int_0^{u_1} dX_{u_0} du_1 dX_{u_2} \\ \int_0^t \int_0^{u_2} \int_0^{u_1} dX_{u_0} dX_{u_1} du_2 & \int_0^t \int_0^{u_2} \int_0^{u_1} dX_{u_0} dX_{u_1} dX_{u_2} \end{pmatrix}$$

In Section 5 we will work with the truncated signature $S(\mathbf{X})_t^{\leq 3}$.

4.1 The Signature Approximation to Volatility

If V has dimension d , let $d_N := \sum_{k=0}^N d^k$ denote the dimension of the truncated tensor algebra $T^N(V)$. The following notation allows us to represent elements of $T^N(V)$ as vectors in \mathbb{R}^{d_N} . Let

$$\mathcal{L} : \{I \mid |I| \leq N\} \rightarrow \{1, \dots, d_N\}$$

be a *labeling* function, that is, a bijection that assigns a unique index to each multi-index I of length at most N . Given any element $\ell = \sum_{|I| \leq N} \ell_I e_I \in T^N(V)$, the map

$$\begin{aligned} \mathbf{vec} : T^N(V) &\rightarrow \mathbb{R}^{d_N} \\ \ell &\mapsto (\ell_{\mathcal{L}^{-1}(1)}, \dots, \ell_{\mathcal{L}^{-1}(d_N)}). \end{aligned}$$

flattens the elements of $T^N(V)$ allowing us to identify tensors with vectors in \mathbb{R}^{d_N} . This makes the use of signature data in linear models or numerical algorithms quite convenient. We now apply this to the truncated signature $\tilde{S}_t(\ell)$.

Assume that the primary process $\mathbf{X} \in \Lambda_T^p(V)$ is obtained as the time-augmented rough path lift of a stochastic process (t, X_t) , where X_t solves an SDE driven by a Brownian motion W_t . In particular, \mathbf{X} is measurable with respect to W and adapted to its natural filtration.

As above, let $f : \Lambda_T^p(V) \rightarrow \mathbb{R}$ be a continuous function with $\sigma_t = f((\mathbf{X}_s)_{s \in [0, t]})$ and define the process $Z_t := \rho W_t + \sqrt{1 - \rho^2} B_t$, where B is a Brownian motion independent of W . Our model is

then

$$d\tilde{S}_t(\ell) = \tilde{S}_t(\ell) \sigma_t(\ell) dZ_t \quad (4.3)$$

$$\sigma_t(\ell) = \sum_{|I| \leq N} \ell_I \langle e_I, S(\mathbf{X})_t^{\leq N} \rangle, \quad (4.4)$$

where the stochastic integral in (4.3) is a well-defined Itô integral, since $\sigma_t(\ell)$ is a predictable process adapted to the filtration of W , and Z is a Brownian motion correlated with W . Recall that $S(\mathbf{X})_t := S(\mathbf{X}^{[t]})_{0,t}$ denotes the signature of the stopped path $\mathbf{X}^{[t]}$.

The solution of equation (4.3) can be expressed in terms of the signature as follows.

Proposition 4.2. *Let $\tilde{S}_t(\ell)$ be the discounted price process defined by (4.3), and assume that $\mathbf{X} \in WG\hat{\Omega}_T^p(V)$ is the time-augmented weakly geometric p -rough path lift of a stochastic process (t, X_t) adapted to a Brownian motion W . Let $Z_t = \rho W_t + \sqrt{1-\rho^2} B_t$, where B is a Brownian motion independent of W . Then, for a given $N \geq 1$, the discounted price process $\tilde{S}_t(\ell)$ admits the representation*

$$\tilde{S}_t(\ell) = S_0 \exp \left(\ell^T Q(t) \ell + \ell^T \int_0^t \mathbf{vec}(S(\mathbf{X})_s^{\leq N}) dZ_s \right),$$

where ℓ^T denotes the transpose of ℓ , and $Q(t)$ is the symmetric matrix defined by

$$Q(t)_{\mathcal{L}(I), \mathcal{L}(J)} := -\frac{1}{2} \left\langle (e_I \sqcup e_J) \otimes e_0, S(\mathbf{X})_t^{\leq 2N+1} \right\rangle.$$

Proof. Rewrite (4.3) as

$$\frac{d\tilde{S}_t(\ell)}{\tilde{S}_t(\ell)} = \sigma_t(\ell) dZ_t.$$

Applying Itô's formula, we have

$$\begin{aligned} d \log(\tilde{S}_t(\ell)) &= \frac{d\tilde{S}_t(\ell)}{\tilde{S}_t(\ell)} + \frac{1}{2} \left(\frac{-1}{\tilde{S}_t(\ell)^2} \right) \sigma_t(\ell)^2 \tilde{S}_t(\ell)^2 dt \\ &= -\frac{1}{2} \sigma_t(\ell)^2 dt + \sigma_t(\ell) dZ_t. \end{aligned}$$

Integrating and rearranging we get

$$\tilde{S}_t(\ell) = S_0 \exp \left(-\frac{1}{2} \int_0^t \sigma_s(\ell)^2 ds + \int_0^t \sigma_s(\ell) dZ_s \right). \quad (4.5)$$

With the notation introduced above, we can express the linear approximation of order N to the volatility as

$$\sigma_t(\ell) = \ell^T \mathbf{vec} \left(S(\mathbf{X})_t^{\leq N} \right).$$

It follows that

$$\sigma_t(\ell)^2 = \left(\ell^T \mathbf{vec} \left(S(\mathbf{X})_t^{\leq N} \right) \right) \left(\ell^T \mathbf{vec} \left(S(\mathbf{X})_t^{\leq N} \right) \right)^T = \ell^T \mathbf{vec} \left(S(\mathbf{X})_t^{\leq N} \right) \mathbf{vec} \left(S(\mathbf{X})_t^{\leq N} \right)^T \ell.$$

Define $\tilde{Q}(t) := \mathbf{vec} \left(S(\mathbf{X})_t^{\leq N} \right) \mathbf{vec} \left(S(\mathbf{X})_t^{\leq N} \right)^T$, which is a symmetric positive semi-definite matrix representing the outer product of the truncated signature vector with itself. We then have

$$\sigma_t(\ell)^2 = \ell^T \tilde{Q}(t) \ell.$$

Note that the elements of $\tilde{Q}(t)$ are

$$\tilde{Q}(t)_{\mathcal{L}(I), \mathcal{L}(J)} = \langle e_I, S(\mathbf{X})_t^{\leq N} \rangle \langle e_J, S(\mathbf{X})_t^{\leq N} \rangle = \langle e_I \sqcup e_J, S(\mathbf{X})_t^{\leq 2N} \rangle.$$

It follows that

$$\begin{aligned} \int_0^t \tilde{Q}(s)_{\mathcal{L}(I)\mathcal{L}(J)} ds &= \int_0^t \langle e_I \sqcup e_J, S(\mathbf{X})_s^{\leq 2N} \rangle ds \\ &= \langle (e_I \sqcup e_J) \otimes e_0, S(\mathbf{X})_t^{\leq 2N+1} \rangle. \end{aligned} \quad (4.6)$$

If we define the matrix $Q(t)$ by

$$Q(t)_{\mathcal{L}(I)\mathcal{L}(J)} := -\frac{1}{2} \langle (e_I \sqcup e_J) \otimes e_0, S(\mathbf{X})_t^{\leq 2N+1} \rangle, \quad (4.7)$$

then the first term in the exponential of (4.5) can be written as

$$-\frac{1}{2} \int_0^t \sigma_s(\ell)^2 ds = \ell^T \left(-\frac{1}{2} \int_0^t \tilde{Q}(s) ds \right) \ell = \ell^T Q(t) \ell.$$

The second term in the exponential is

$$\int_0^t \sigma_s(\ell) dZ_s = \ell^T \int_0^t \text{vec}(S(\mathbf{X})_s^{\leq N}) dZ_s,$$

which concludes the proof. \square

Since $\tilde{Q}(t)$ is positive semi-definite by construction, it follows that $Q(t)$ is negative semi-definite. That is, for every $\ell \in \mathbb{R}^{d_N}$,

$$\ell^T Q(t) \ell \leq 0.$$

As the Cholesky decomposition applies to positive semi-definite matrices, $-Q(t)$ admits a Cholesky decomposition $U(t)^T U(t)$. We can therefore write

$$\ell^T Q(t) \ell = -\|U(t)\ell\|_2^2.$$

Note that it is cheaper to compute $\|U(t)\ell\|_2^2$ than $\ell^T Q(t) \ell$.

Remark 4.3. From (4.7) we see that $Q(t)$ depends on the signature $S(\mathbf{X})_t$ up to level $2N + 1$.

If the signature is truncated at level $N = 3$, then $\tilde{Q}(t)$ is a 15×15 -matrix, whose elements are of the type $\langle e_I, S(\mathbf{X})_t^{\leq 3} \rangle$, where the 15 basis elements are

$$\{1, e_0, e_1, e_{00}, e_{01}, e_{10}, e_{11}, e_{000}, e_{001}, e_{010}, e_{011}, e_{100}, e_{101}, e_{110}, e_{111}\}.$$

With the above ordering, $\mathcal{L}(e_{01}) = 5$ and $\mathcal{L}(e_{111}) = 15$. The $(15, 5)$ -entry of matrix $\tilde{Q}(t)$ is therefore

$$\tilde{Q}(t)_{15,5} = \langle e_{111}, S(\mathbf{X})_t^{\leq 3} \rangle \langle e_{01}, S(\mathbf{X})_t^{\leq 3} \rangle.$$

By (4.6),

$$\int_0^t \tilde{Q}(s)_{15,5} ds = \langle (e_{111} \sqcup e_{01}) \otimes e_0, S(\mathbf{X})_t^{\leq 7} \rangle,$$

where

$$\begin{aligned} (e_{111} \sqcup e_{01}) \otimes e_0 &= (e_{11101} + 2e_{11011} + 3e_{10111} + 4e_{01111}) \otimes e_0 \\ &= e_{111010} + 2e_{110110} + 3e_{101110} + 4e_{011110}, \end{aligned}$$

which includes basis elements of tensor spaces of higher dimensions. In particular, to compute the matrix $Q(t)$, we see from (4.7) that its entries $\langle (e_I \sqcup e_J) \otimes e_0, S(\mathbf{X})_t^{\leq 2N+1} \rangle$ live in a space of dimension $2^{(2N+1)+1} - 1$.

In our particular case, $2N + 1 = 7$, so $Q(t)$ depends on signature entries in $T^{\leq 7}(\mathbb{R} \oplus V)$, a space of dimension $2^8 - 1 = 255$. In other words, to populate a 15×15 matrix we need to fetch its elements from the entries of a 255×255 matrix.

4.2 Calibration

Assume we have a theoretical model for the evolution of a discounted asset price, parameterized by θ , and given by

$$d\tilde{S}_t^\theta = \tilde{S}_t^\theta \sigma_t^\theta dZ_t,$$

where σ_t^θ is the volatility process associated with the parameter θ , and Z_t is as in (4.3). For a given θ , we can compute the price of a European call option with strike K and maturity T as

$$C(K, T, \theta) = e^{-rT} \mathbb{E}[(S_T^\theta - K)_+] = \mathbb{E}[(\tilde{S}_T^\theta - e^{-rT} K)_+].$$

Let $\{C^{\text{mkt}}(K_i, T_i)\}_{i=1}^N$ denote the observed market prices for varying strikes and maturities. If there exists a parameter θ^* such that the model perfectly describes the real dynamics of the asset, then

$$C^{\text{mkt}}(K_i, T_i) = C(K_i, T_i, \theta^*) \quad \text{for all } i.$$

While this exact match is unlikely in practice, our goal is to find a parameter configuration θ that minimizes the discrepancy between the model and market prices. We thus consider the least squares loss function

$$L(\theta) = \sum_{i=1}^N \gamma_i (C^{\text{mkt}}(K_i, T_i) - C(K_i, T_i, \theta))^2,$$

where $\gamma_i > 0$ are user-specified weights.

In the case of signature-based models, the role of the parameter θ is played by a vector $\ell \in \mathbb{R}^{d_N}$, where d_N is the dimension of the truncated signature space. The corresponding loss function becomes

$$L(\ell) = \sum_{i=1}^N \gamma_i (C^{\text{mkt}}(K_i, T_i) - C(K_i, T_i, \ell))^2. \quad (4.8)$$

Recall that the value of the signature-driven price process $\tilde{S}_t(\ell)$ at maturity $t = T$ is given by

$$\tilde{S}_T(\ell)(\omega) = S_0 \exp \left(-\|U(T)(\omega) \ell\|_2^2 + \ell^T \int_0^T \mathbf{vec} \left(S(\mathbf{X})_t^{\leq N}(\omega) \right) dZ_t \right), \quad (4.9)$$

where $U(T)(\omega)$ is the Cholesky factor associated with $-Q(T)$ on sample path ω , and $S(\mathbf{X})_t^{\leq N}$ is the truncated signature of the primary process \mathbf{X} up to level N .

4.3 The Algorithm

We now detail the computational pipeline used to minimize the loss function $L(\ell)$ defined in (4.8). The approach proceeds in two main phases: the generation of synthetic option prices from the model, and the calibration of ℓ via numerical optimization.

The starting point is equation (4.9), which is used to simulate discounted stock prices \tilde{S}_T at four different maturities $T \in \{0.1, 0.6, 1.1, 1.6\}$. For each T and strike $K \in \{90, 95, 100, 105, 110\}$, we compute the corresponding option price using Monte Carlo simulation. In total, this yields 20 model-generated option prices

$$C(K_i, T_i, \ell) \approx \frac{1}{n_{\text{MC}}} \sum_{j=1}^{n_{\text{MC}}} \left(\tilde{S}_{T_i}(\ell)(\omega_j) - e^{-rT_i} K_i \right)_+,$$

$i = 1, \dots, 20$, where n_{MC} is the number of Monte Carlo samples, and each ω_j denotes a sample path. Since this simulation must be repeated for many ℓ values during optimization, recomputing $U(T)$ and the stochastic integrals $\int_0^T \mathbf{vec}(S(\mathbf{X})_t^{\leq N}) dZ_t$ represents a first computational bottleneck.

For the calibration, we use as ground truth the synthetic market prices $\{C^{\text{mkt}}(K_i, T_i)\}_{i=1}^{20}$ generated in Alòs et al. (2015) under the assumption that the market follows Heston-type dynamics. Thus, we are assuming for benchmarking purposes that *the market is Heston*.

Unlike Alòs et al. (2015), which estimates the Heston parameters via a second-order asymptotic expansion, the signature-based approach directly minimizes the discrepancy between model-generated and market prices via:

$$L(\ell) = \sum_{i=1}^{20} \gamma_i \left(C^{\text{mkt}}(K_i, T_i) - C(K_i, T_i, \ell) \right)^2,$$

where the weights γ_i are proportional to the inverse Vega of each option. This minimization process constitutes the second bottleneck.

Once the optimal coefficient vector ℓ^* is obtained, we produce three sets of option prices:

- $\{C^{\text{mkt}}(K_i, T_i)\}$, the synthetic "market" prices,
- $\{C(K_i, T_i, \ell^*)\}$, the signature model prices,
- $\{C^{\text{ASV}}(K_i, T_i)\}$, the prices using the second-order approximation in Alòs et al. (2015).¹

From these prices, we compute three implied volatility surfaces using the Black-Scholes formula:

- $\{IV^{\text{mkt}}(K_i, T_i)\}$, from the "market" prices,
- $\{IV^{\text{SIG}}(K_i, T_i, \ell^*)\}$, from the signature model prices,
- $\{IV^{\text{ASV}}(K_i, T_i)\}$, from the second-order approximation prices.

These surfaces are compared in Section 5. We now describe the algorithm in detail.

1. **Simulate sample paths.** Generate n_{MC} Monte Carlo paths for the Brownian motions W and B using Gaussian increments. Construct $Z = \rho W + \sqrt{1 - \rho^2} B$, and simulate the process X using an Euler scheme. Using X , construct the primary path \mathbf{X} , and for each path:

- compute the truncated signature $S(\mathbf{X})_T^{\leq 2N+1}$,
- evaluate the stochastic integral $\int_0^T \text{vec}(S(\mathbf{X})_t^{\leq N}) dZ_t$.

2. **Assemble the matrix $Q(T)$.** For each sample path, compute the symmetric matrix

$$Q(T)_{\mathcal{L}(I), \mathcal{L}(J)} = -\frac{1}{2} \left\langle (e_I \sqcup e_J) \otimes e_0, S(\mathbf{X})_T^{\leq 2N+1} \right\rangle,$$

and perform a Cholesky decomposition of $-Q(T)$ to obtain $U(T)$.

3. **Optimize the loss.** Initialize $\ell \in \mathbb{R}^{d_N}$ and iterate the following steps until convergence:

- (a) For each path ω_j , evaluate

$$\tilde{S}_T(\ell)(\omega_j) = S_0 \exp \left(-\|U(T)(\omega_j) \ell\|_2^2 + \ell^T \int_0^T \text{vec}(S(\mathbf{X})_t^{\leq N}(\omega_j)) dZ_t \right).$$

- (b) Compute $C(K_i, T_i, \ell)$ as the Monte Carlo average over ω_j .

- (c) Evaluate $L(\ell)$ and update ℓ using a numerical optimizer.

¹In what follows, the superscript ASV (from the authors' surnames) refers to results based on the method developed in Alòs et al. (2015), while SIG denotes results from the signature-based approach.

Implementation details. All experiments in Section 5 use $n_{\text{MC}} = 800,000$ Monte Carlo paths and signature truncation level $N = 3$. Brownian increments are generated via standard Gaussian sampling, and X is simulated using an Euler discretization.

Signatures are computed using a vectorized version of Peter Foster’s code², adapted for GPU acceleration. Optimization of $L(\ell)$ is done using SciPy’s `minimize` function with the L-BFGS-B method (tolerance 10^{-8}), and with box constraints on ℓ to accelerate convergence.

All computations were carried out on a consumer desktop with 128 GB RAM and an NVIDIA RTX 3080 Ti GPU, without access to specialized computing clusters.

5 Numerical Analysis

In this section, we compare the performance of the signature-based method introduced in Section 4 with the parametric calibration approach of Alòs et al. (2015). Before presenting the results, we highlight an important structural property of signatures that will serve as a diagnostic for numerical approximation quality.

Proposition 5.1 (Factorial Decay). *Let $X : [0, T] \rightarrow \mathbb{R}^d$ be a path of finite p -variation for some $p \geq 1$, and let $\mathbf{X} \in W\hat{G}\hat{\Omega}_T^p(\mathbb{R}^d)$ denote its time-augmented weakly geometric rough path lift. Then for all $k \geq 1$, the k -th level satisfies*

$$\|\mathbf{X}_{s,t}^k\| \leq \frac{C(X)^k}{k!},$$

for some constant $C(X) > 0$ depending on X , uniformly over all $(s, t) \in \Delta_T$, and for any tensor norm on $(\mathbb{R}^d)^{\otimes k}$.

This factorial decay follows from the multiplicative (group-like) structure and the control provided by the p -variation norm. In practice, it serves as a valuable check: the magnitudes of the iterated integrals should decay rapidly with k , and deviations from this pattern can signal numerical instability or truncation issues. See Lyons (1998) and (Friz and Victoir, 2010, Thm. 10.35) for proofs and generalizations.

For paths of bounded variation, a stronger estimate holds:

$$\|\mathbf{X}_{s,t}^k\| \leq \frac{1}{k!} \|\mathbf{X}\|_{1\text{-var}}^k,$$

as noted in Fermanian (2021). This bound is exact for signatures of bounded variation paths. Although it does not hold for arbitrary p -rough paths, it remains relevant numerically, since signature approximations are typically based on interpolated (and hence BV) paths.

5.1 Calibration Setup. The Uncorrelated Case.

As the signature-based approach learns volatility directly from a *primary noise*, we first tested this learning mechanism using a Ornstein–Uhlenbeck process. However, to compare fairly with the parametric calibration in Alòs et al. (2015), which is derived under Heston dynamics, we use a Heston process as the primary driver for both approaches.

The market model in Alòs et al. (2015) is given by:

$$\begin{aligned} dS_t &= rS_t dt + \sigma_t S_t d(\rho W_t + \sqrt{1 - \rho^2} B_t), \\ d\sigma_t^2 &= \kappa(\theta - \sigma_t^2) dt + \nu \sqrt{\sigma_t^2} dW_t, \end{aligned}$$

with $S_0 = 100$, $\sigma_0 = 0.2$, $\nu = 0.3$, $\kappa = 3$, and $\theta = 0.09$.

²github.com/pafoster/path_signatures_introduction

We first consider the uncorrelated case $\rho = 0$. The calibrated parameters obtained with the second-order approximation method in Alòs et al. (2015) are:

Parameter	True Value	Calibrated Value
σ_0	0.2	0.200013
ν	0.3	0.307340
κ	3	2.998598
θ	0.09	0.089960
ρ	0	0.000000

Table 1: Calibrated parameters from Alòs et al. (2015) with $\rho = 0$.

Using these parameters, we compute option prices and invert the Black-Scholes formula to reconstruct the implied volatility surface. We will denote these implied volatilities by IV^{ASV} .

Signature-Based Calibration. To calibrate the signature-based model, we consider 20 option prices $C(K_i, T_i)$ at maturities $\{0.1, 0.6, 1.1, 1.6\}$ and strikes $\{90, 95, 100, 105, 110\}$. The primary process X follows a Heston SDE with parameters $X_0 = 0.1$, $\nu = 0.2$, $\kappa = 2$, and $\theta = 0.15$.

Volatility is modeled as:

$$\sigma_t(\ell) = \langle \ell, S(\mathbf{X})_t^{\leq 3} \rangle,$$

where $S(\mathbf{X})_t^{\leq 3}$ is the truncated signature of the time-augmented path $\hat{X}_t = (t, X_t)$. The loss function to minimize is:

$$L(\ell) = \sum_{i=1}^{20} \gamma_i \left(C^{\text{mkt}}(K_i, T_i) - C(K_i, T_i, \ell) \right)^2, \quad (5.1)$$

where γ_i is set as the inverse Vega of the i -th option.

All computations are run with $n_{\text{MC}} = 800,000$ Monte Carlo samples. Since computing the matrix $Q(T)$ involves terms up to level $2N + 1 = 7$, this requires evaluating signatures in a space of dimension $2^8 - 1 = 255$. As mentioned earlier, each 15×15 matrix $Q(T)$ depends on a corresponding 255×255 matrix, making it a computationally intensive step of the algorithm.

Calibration Results. The optimal coefficient vector minimizing $L(\ell)$ is:

$$\begin{aligned} \ell^* = & (0.201202133, 0.142660997, 1.08471290, -0.297312378, -0.0293435325, -0.0422317187, \\ & 9.25090162 \times 10^{-4}, 0.293103687, -0.0143435573, -0.0134285652, -1.64737083 \times 10^{-3}, \\ & -2.89883092 \times 10^{-3}, -5.72798006 \times 10^{-4}, -1.93045420 \times 10^{-3}, -1.84406803 \times 10^{-4}). \end{aligned}$$

Recall that

$$\sigma_t(\ell) = \ell_0 + \ell_0 t + \ell_1 X_t + \ell_{00} t^2 + \ell_{01} \int_0^t s dX_s + \ell_{10} \int_0^t X_s ds + \ell_{11} \int_0^t X_s dX_s + \ell_{000} \frac{t^3}{6} + \dots$$

The coefficient $\ell_1 \approx 1.085$ confirms that the model has learned a strong linear dependence on X_t , consistent with the Heston structure. Likewise, $\ell_0 \approx 0.201$ is close to the initial volatility $\sigma_0 = 0.2$.

The minimum value of the loss function $L(\ell)$ obtained during calibration was 1.05×10^{-4} , indicating a good fit to market prices. From the simulated option prices we compute the implied volatilities, which we denote by IV^{SIG} .

To evaluate the quality of the approximation in implied volatilities, we computed the errors

$$\begin{aligned} e_i^{\text{SIG}} &:= |IV^{\text{SIG}}(K_i, T_i) - IV^{\text{mkt}}(K_i, T_i)| \\ e_i^{\text{ASV}} &:= |IV^{\text{ASV}}(K_i, T_i) - IV^{\text{mkt}}(K_i, T_i)| \end{aligned}$$

for all 20 option contracts (K_i, T_i) . A full breakdown of the implied volatilities and error comparisons is provided in Appendix A.

The two methods yield results of comparable quality, with both achieving high calibration accuracy. In 15 out of the 20 implied volatilities, the absolute error difference between the signature-based (SIG) and asymptotic (ASV) methods is less than 0.0005, indicating that they are effectively of the same magnitude. In several of these cases, the SIG method even outperforms the ASV approach. This highlights the robustness of the signature-based model, which is able to learn the structure of the implied volatility surface without relying on any parametric assumptions. Figure 1 shows a visual comparison between the two surfaces.

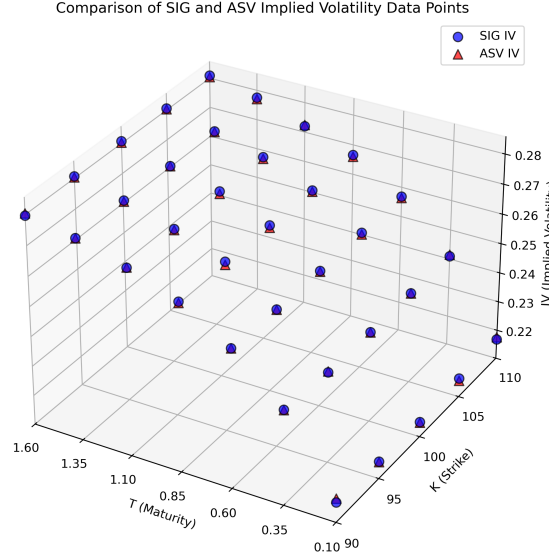


Figure 1: Comparison of implied volatility surfaces: signature-based vs. second-order expansion.

Figures 2–5 plot the volatility smiles across strikes for each maturity.

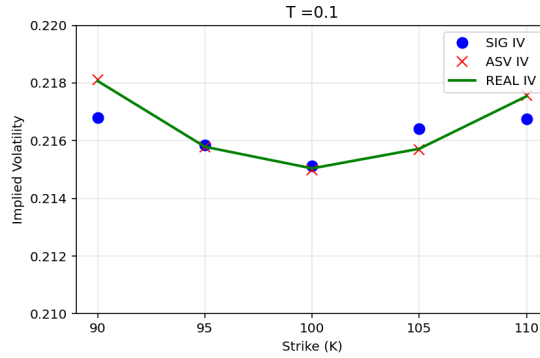


Figure 2: Volatility smiles for $T = 0.1$

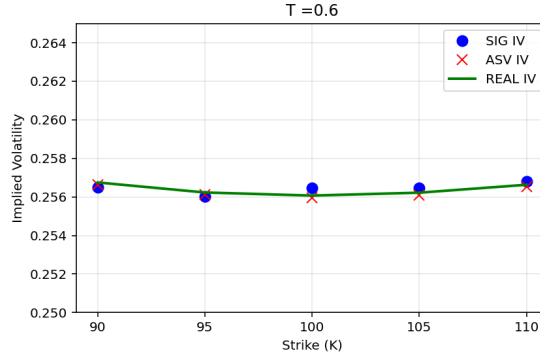


Figure 3: Volatility smiles for $T = 0.6$

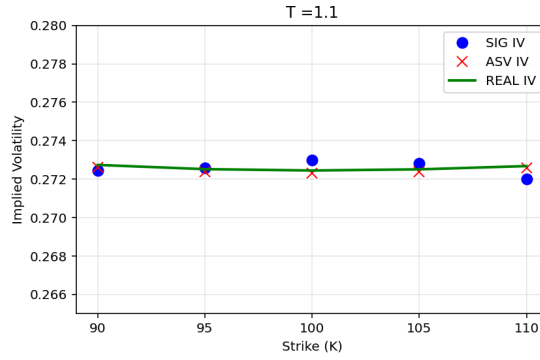


Figure 4: Volatility smiles for $T = 1.1$

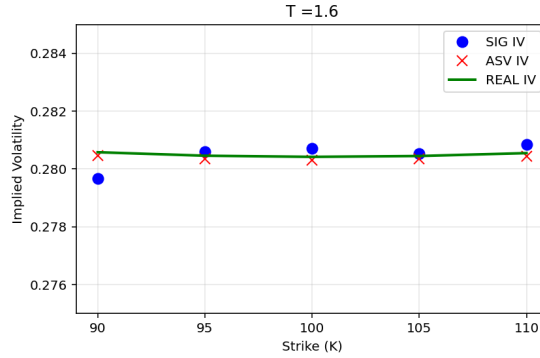


Figure 5: Volatility smiles for $T = 1.6$

As the loss function (5.1) aggregates squared errors across all observed option prices, the global minimum reflects a trade-off: some option prices may be matched very accurately, while others may show larger deviations. To better understand this effect, it is natural to investigate whether calibration accuracy improves when the model is fit to each maturity *smile* independently.

Figure 5.1 illustrates this experiment. We recalibrate the signature-based model separately for each maturity, using only the five corresponding strike prices. The resulting implied volatility smiles demonstrate that the signature method is highly effective at capturing the local structure of the volatility surface, yielding an even more accurate fit than in the joint calibration.

This suggests that local calibration with the signature method can offer a flexible and precise alternative to global parametric approaches—especially when volatility smiles exhibit strong maturity dependence.

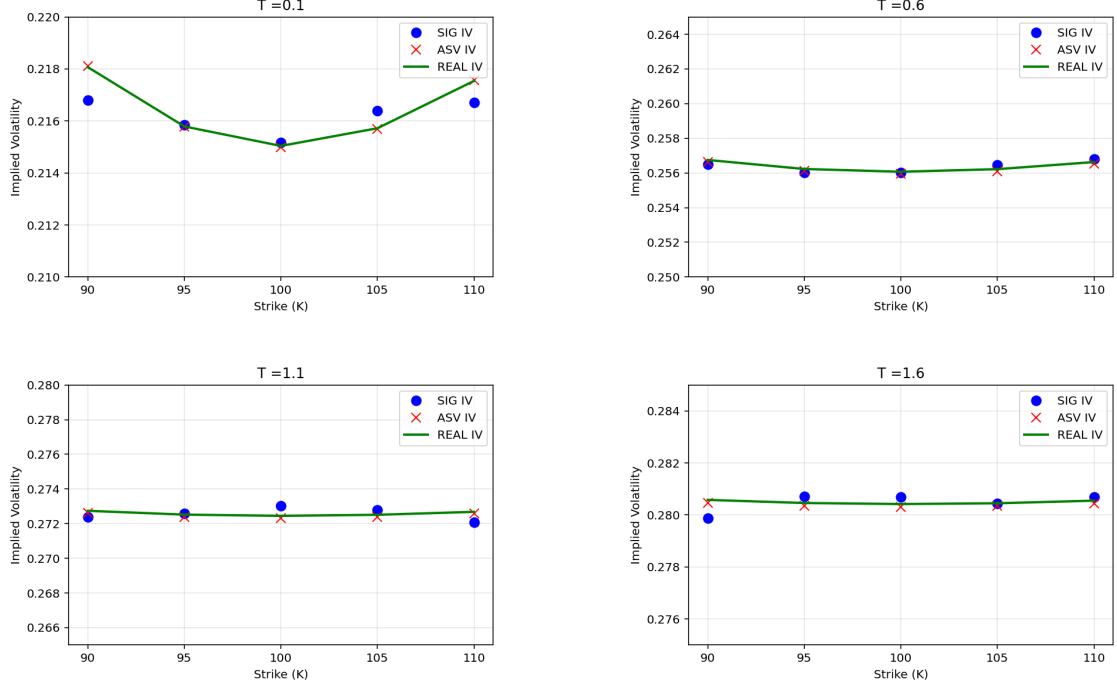


Figure 6: Separate smile calibration.

5.2 The Correlated Case

We now consider the setting where the market exhibits correlation between the asset price and the volatility process. Specifically, we assume the asset dynamics are governed by the following Heston model

$$dS_t = rS_t dt + \sigma_t S_t d\left(\rho W_t + \sqrt{1 - \rho^2} B_t\right)$$

$$d\sigma_t^2 = \kappa(\theta - \sigma_t^2) dt + \nu \sqrt{\sigma_t^2} dW_t,$$

with $S_0 = 100$, $\sigma_0 = 0.2$, $\nu = 0.3$, $\kappa = 3$, $\theta = 0.09$, and correlation $\rho = -0.5$.

Using the second-order approximation of Alòs et al. (2015), the calibrated parameters are:

Parameter	True Value	Calibrated Value
σ_0	0.2	0.200016
ν	0.3	0.290138
κ	3	2.973728
θ	0.09	0.090022
ρ	-0.5	-0.504084

Table 2: Calibrated parameters from Alòs et al. (2015) with $\rho = -0.5$.

As in the uncorrelated case, we compute the option prices with these parameters, and we invert them to obtain the implied volatility surface IV^{ASV} .

Signature-Based Calibration. For the signature-based approach, we let $X_0 = 0.25$, $\nu = 0.35$, $\kappa = 3.3$, $\theta = 0.15$ and $\rho = -0.5$ be the parameters of the *primary* Heston process X , and we approximate the volatility by the truncated signature

$$\sigma_t(\ell) = \langle \ell, S(\mathbf{X})_t^{\leq 3} \rangle.$$

The loss function remains as in (5.1). The optimal coefficient vector is

$$\begin{aligned} \ell^* = & (-0.195158212, -0.250867130, -0.125195785, 0.606113847, -0.303740047, \\ & 0.347580926, 0.136816382, -0.664746087, 0.563172308, 0.033241841, \\ & 0.029376982, 0.019240593, -0.065104522, 3.67 \times 10^{-5}, -8.94 \times 10^{-3}). \end{aligned}$$

Whereas in the uncorrelated setting, the optimizer happened to find a parameterization close to the true process, in the correlated case it settled on a different (but still effective) minimizer. The minimum value of the loss function $L(\ell)$ was 1.46×10^{-3} , indicating a strong overall fit to market prices, albeit slightly less precise than in the uncorrelated case. To assess pointwise accuracy in implied volatility, we compute the absolute errors

$$\begin{aligned} e_i^{\text{SIG}} &:= |IV^{\text{SIG}}(K_i, T_i) - IV^{\text{mkt}}(K_i, T_i)|, \\ e_i^{\text{ASV}} &:= |IV^{\text{ASV}}(K_i, T_i) - IV^{\text{mkt}}(K_i, T_i)|, \end{aligned}$$

for each of the 20 contracts (K_i, T_i) . A detailed breakdown of implied volatilities and error comparisons is provided in Appendix B.

As in the uncorrelated case, both methods deliver comparably accurate results, though the overall precision is slightly lower when correlation is introduced. In half of the cases, the absolute error difference between the signature-based (SIG) and asymptotic (ASV) methods is below 0.001, and in several of these, the SIG approach yields the smaller error. These findings underscore the ability of the signature-based model to capture the structure of the implied volatility surface with high fidelity, even under correlated dynamics. Figure 7 provides a visual comparison of the two calibrated surfaces.

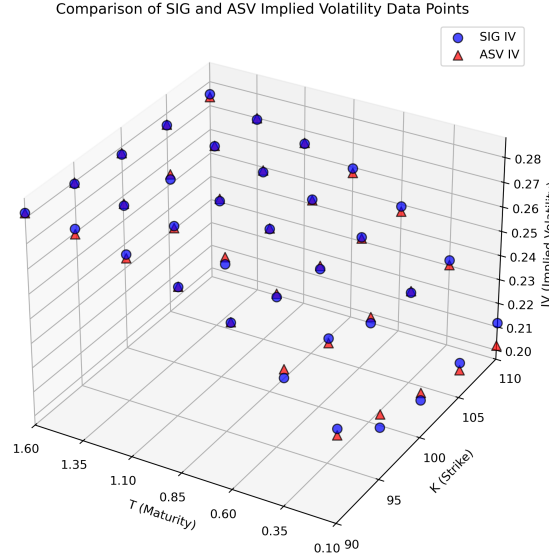


Figure 7: Comparison of implied volatility surfaces: SIG (signature), ASV (second-order).

Figures 8–11 show the volatility smiles at each maturity. As before, the solid curve represents the true market implied volatilities, crosses mark the second-order approximation (ASV), and dots mark the signature-based estimates (SIG).

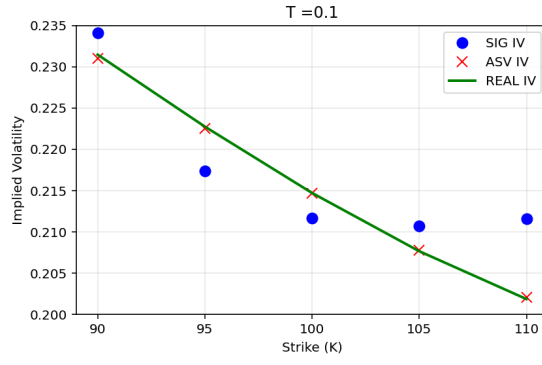


Figure 8: Volatility smile at $T = 0.1$.

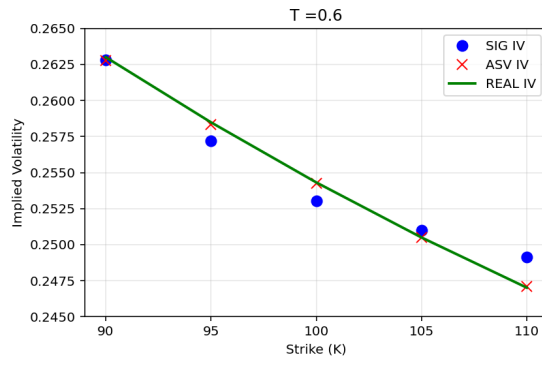


Figure 9: Volatility smile at $T = 0.6$.

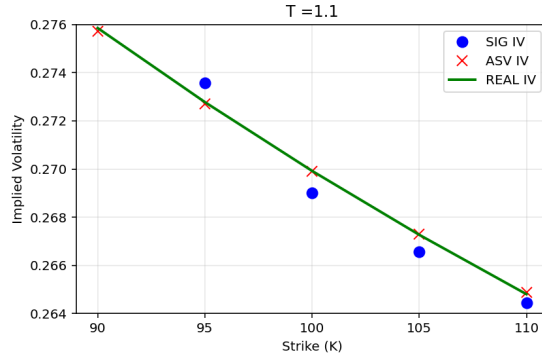


Figure 10: Volatility smile at $T = 1.1$.

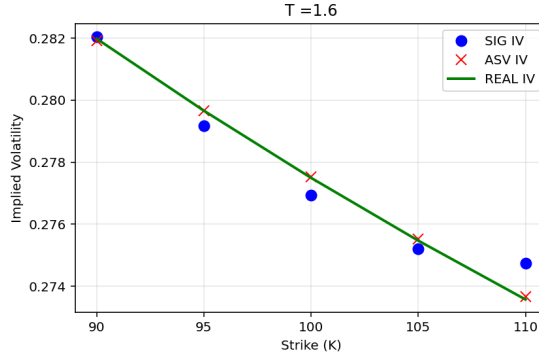


Figure 11: Volatility smile at $T = 1.6$.

5.3 Calibration with a Rough Bergomi Primary Process

The second-order approximation in Alòs et al. (2015) provides an effective tool for calibrating implied volatility surfaces, but assumes that *the market is Heston*. In contrast, the signature-based method makes no structural assumptions about the underlying stochastic volatility, offering greater flexibility and robustness across models.

To demonstrate this flexibility, we calibrate our signature-based model using synthetic data generated from the *rough Bergomi model*, which is fundamentally different from Heston. Since the asymptotic method in Alòs et al. (2015) is not designed to accommodate rough volatility, we omit it from this section's comparison and focus solely on the signature method.

The stock price is now driven by the dynamics:

$$\begin{aligned} dS_t &= rS_t dt + \sigma_t S_t d\left(\rho W_t + \sqrt{1 - \rho^2} B_t\right), \\ \sigma_t^2 &= \sigma_0^2 \exp\left(\eta W_t^H - \frac{1}{2}\eta^2 t^{2H}\right), \end{aligned}$$

where W_t^H is a Volterra-type fractional Brownian motion:

$$W_t^H := \int_0^t K_H(t, s) dW_s, \quad \text{with } K_H(t, s) = \sqrt{2H} (t - s)^{H - \frac{1}{2}} \mathbf{1}_{[0, t]}(s),$$

for $H \in (0, 1)$ and $\eta > 0$.

We simulate this model with $\sigma_0 = 0.2$, $\eta = 0.5$, and Hurst exponent $H = 0.1$. Although we also tested values $H = 0.3, 0.7$, and 0.9 , we report here only the most challenging case $H = 0.1$.

As primary noise, we take a Heston-type process X : that is, we assume the model does not *know* the market is rough. In particular, we let:

$$dX_t = \kappa(\theta - X_t) dt + \nu \sqrt{X_t} dW_t,$$

with $X_0 = 0.1$, $\kappa = 2$, $\theta = 0.15$, $\nu = 0.2$ and $\rho = 0$. We define the volatility model as:

$$\sigma_t(\ell) = \langle \ell, S(\mathbf{X})_t^{\leq 3} \rangle,$$

where \mathbf{X} is the time-augmented rough path lift of (t, X_t) .

The optimal parameter vector ℓ^* obtained by minimizing the loss function (5.1) is:

$$\begin{aligned} \ell^* &= (0.196633, -0.0605951, 0.571142, 0.103006, 9.90463 \times 10^{-3}, 0.0135898, \\ &\quad -2.32462 \times 10^{-4}, -0.101164, 4.35842 \times 10^{-3}, 3.91499 \times 10^{-3}, \\ &\quad 6.56794 \times 10^{-4}, 4.54101 \times 10^{-5}, 1.69383 \times 10^{-4}, 6.53983 \times 10^{-4}, 6.59773 \times 10^{-5}). \end{aligned}$$

The minimum value of the loss function was 9.74×10^{-5} , which is significantly smaller than in the previous experiments with Heston-generated data—indicating that the signature model fits the rough Bergomi surface even more accurately.

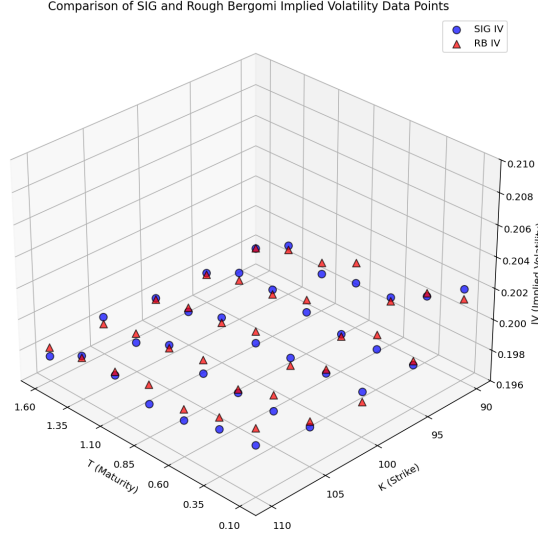


Figure 12: Implied Volatility Surface: Rough Bergomi (market) vs. Signature Model ($H = 0.1$).

Notably, the leading coefficient $\ell_0 \approx 0.1966$ is close to $\sigma_0 = 0.2$, and the remaining coefficients exhibit approximate factorial decay. This confirms that the model learns both the shape and scale of the implied volatility surface, even when trained on data generated by a rough volatility model using a Heston-based primary noise.

For completeness, the detailed comparison between the signature-based implied volatilities and the rough Bergomi “market” volatilities is given in Appendix C. Note how the pointwise errors are extremely small across all maturities and strikes.

6 Conclusions

This paper provides a detailed comparison between two different approaches to the calibration of implied volatility surfaces: the second-order asymptotic expansion method of Alòs et al. (2015), and a data-driven method based on signatures of rough paths. Each methodology has its strengths, and the comparison sheds light on the trade-offs between structure, flexibility, and computational complexity.

The method of Alòs et al. (2015) builds on a model-specific framework—in particular, the Heston model—and derives calibration formulas from an asymptotic expansion of implied volatility using tools from Malliavin calculus. When the true market dynamics are indeed Heston (as in our benchmark simulations), this approach achieves excellent accuracy with low computational cost. The calibration enjoys a low-dimensional parameter space and relies only on a limited subset of the implied volatility surface, making it robust and highly efficient.

By contrast, the signature-based method does not assume any parametric form for the volatility. Instead, volatility is modeled as a linear functional of the signature of a *primary* process, which can be freely chosen. The method is universal and flexible: it learns the volatility structure directly from the data, without requiring explicit assumptions about the underlying dynamics. This model-agnostic property is particularly valuable in settings where traditional models fail to capture key features, such as roughness, skew, or term structure nonlinearity.

Our numerical experiments illustrate this flexibility clearly. When the market is simulated

under Heston dynamics, the signature-based model achieves a calibration accuracy comparable to the model-specific asymptotic method, with implied volatility errors typically below 10^{-3} . Moreover, when the market is driven by a rough Bergomi model, the signature approach maintains excellent performance, with errors of similar magnitude and stable coefficients. The ability of the signature model to learn the surface even in this more complex setting highlights its strength as a model-independent calibration tool.

From a computational perspective, the full-surface calibration using signatures, with truncation at level $N = 3$, takes approximately 90 minutes on a standard desktop (128 GB RAM, RTX 3080 Ti GPU). Local calibration of individual volatility smiles (per maturity) completes in under 4 minutes, making the approach practical for both batch and incremental use cases. While we experimented with deeper signatures (e.g., $N = 4$) and higher-order interpolation schemes (e.g., cubic splines), the marginal gains in accuracy were minimal compared to the added computational cost. The results reported here represent an optimal balance between precision and efficiency.

It is worth noting that the computation of the matrix $Q(t)$ (required for pricing) involves signature terms up to level $2N + 2$, leading to high-dimensional linear algebra operations. Nonetheless, the factorial decay property of the signature ensures numerical stability, and modern GPU-based linear algebra routines mitigate the associated costs.

In summary, while the second-order asymptotic method of Alòs et al. (2015) remains a highly effective and computationally elegant solution when its assumptions hold, the signature-based framework offers a compelling alternative for more general settings. It combines theoretical rigor with practical flexibility, and its compatibility with modern learning techniques places it as a promising direction for future volatility modeling and calibration.

Appendices

A Detailed Error Comparison: Uncorrelated Case

The table below compares the implied volatilities produced by the signature-based model (IV^{SIG}) and the second-order asymptotic method of Alòs et al. (2015) (IV^{ASV}) against the market-implied volatility (IV^{mkt}), for all (K, T) combinations. Errors are given by e^{SIG} and e^{ASV} , respectively.

T	K	IV^{SIG}	IV^{ASV}	IV^{mkt}	e^{SIG}	e^{asv}
0.1	90	0.21680	0.21811	0.21807	0.00127	0.00004
0.1	95	0.21586	0.21577	0.21579	0.00007	0.00002
0.1	100	0.21513	0.21500	0.21504	0.00009	0.00005
0.1	105	0.21641	0.21569	0.21572	0.00069	0.00003
0.1	110	0.21676	0.21757	0.21754	0.00078	0.00003
0.6	90	0.25651	0.25665	0.25675	0.00024	0.00010
0.6	95	0.25602	0.25612	0.25623	0.00021	0.00012
0.6	100	0.25602	0.25595	0.25607	0.00005	0.00012
0.6	105	0.25648	0.25610	0.25622	0.00026	0.00012
0.6	110	0.25681	0.25652	0.25663	0.00019	0.00010
1.1	90	0.27244	0.27262	0.27274	0.00029	0.00011
1.1	95	0.27260	0.27239	0.27252	0.00008	0.00012
1.1	100	0.27300	0.27232	0.27245	0.00055	0.00012
1.1	105	0.27282	0.27239	0.27251	0.00031	0.00012
1.1	110	0.27200	0.27257	0.27268	0.00069	0.00012
1.6	90	0.27968	0.28047	0.28058	0.00089	0.00011
1.6	95	0.28060	0.28034	0.28046	0.00014	0.00012
1.6	100	0.28071	0.28030	0.28042	0.00029	0.00012
1.6	105	0.28053	0.28034	0.28045	0.00008	0.00012
1.6	110	0.28086	0.28044	0.28055	0.00031	0.00011

Table 3: Detailed comparison of implied volatilities and errors for the uncorrelated case ($\rho = 0$).

B Detailed Error Comparison: Correlated Case

T	K	IV^{SIG}	IV^{ASV}	IV^{mkt}	e^{SIG}	e^{ASV}
0.1	90	0.23407	0.23099	0.23146	0.00261	0.00046
0.1	95	0.21740	0.22252	0.22275	0.00535	0.00023
0.1	100	0.21165	0.21471	0.21472	0.00307	0.00002
0.1	105	0.21071	0.20779	0.20767	0.00304	0.00013
0.1	110	0.21160	0.20206	0.20188	0.00972	0.00018
0.6	90	0.26282	0.26276	0.26300	0.00018	0.00024
0.6	95	0.25718	0.25834	0.25848	0.00130	0.00014
0.6	100	0.25304	0.25426	0.25431	0.00127	0.00005
0.6	105	0.25100	0.25051	0.25049	0.00051	0.00002
0.6	110	0.24916	0.24708	0.24701	0.00215	0.00008
1.1	90	0.27730	0.27572	0.27584	0.00146	0.00012
1.1	95	0.27358	0.27271	0.27277	0.00081	0.00006
1.1	100	0.26901	0.26991	0.26992	0.00091	0.00001
1.1	105	0.26657	0.26731	0.26726	0.00069	0.00004
1.1	110	0.26444	0.26488	0.26480	0.00036	0.00008
1.6	90	0.28205	0.28192	0.28197	0.00007	0.00005
1.6	95	0.27918	0.27965	0.27966	0.00047	0.00001
1.6	100	0.27693	0.27752	0.27749	0.00056	0.00003
1.6	105	0.27520	0.27553	0.27547	0.00027	0.00006
1.6	110	0.27475	0.27367	0.27357	0.00118	0.00010

Table 4: Implied volatility error comparison for the correlated case ($\rho = -0.5$).

C Error Comparison for Rough Bergomi with $H = 0.1$

T	K	IV^{SIG}	IV^{rB}	error
0.1	90	0.20195	0.20131	0.00064
0.1	95	0.19882	0.19908	0.00026
0.1	100	0.19891	0.19826	0.00064
0.1	105	0.19852	0.19888	0.00036
0.1	110	0.19927	0.20033	0.00106
0.6	90	0.19916	0.19891	0.00025
0.6	95	0.19847	0.19832	0.00015
0.6	100	0.19869	0.19819	0.00050
0.6	105	0.19824	0.19846	0.00021
0.6	110	0.19832	0.19903	0.00071
1.1	90	0.19848	0.19923	0.00075
1.1	95	0.19911	0.19880	0.00031
1.1	100	0.19898	0.19864	0.00034
1.1	105	0.19893	0.19873	0.00020
1.1	110	0.19876	0.19899	0.00023
1.6	90	0.19791	0.19803	0.00012
1.6	95	0.19799	0.19788	0.00011
1.6	100	0.19798	0.19789	0.00008
1.6	105	0.19844	0.19798	0.00046
1.6	110	0.19761	0.19818	0.00057

Table 5: Absolute errors $|IV^{\text{SIG}} - IV^{\text{rB}}|$ for the rough Bergomi case ($H = 0.1$).

References

- Alòs, E., De Santiago, R., and Vives, J. (2015). Calibration of stochastic volatility models via second-order approximation: The Heston case. *International Journal of Theoretical and Applied Finance*, 18(06):1550036.
- Alòs, E., León, J., and Vives, J. (2007). On the short-time behavior of the implied volatility for jump-diffusion models with stochastic volatility. *Finance and Stochastics*, 11:571–589.
- Alòs, E. (2012). A decomposition formula for option prices in the Heston model and applications to option pricing approximation. *Finance and Stochastics*, 16(3):403–422.
- Antonelli, F. and Scarlatti, S. (2009). Pricing options under stochastic volatility: A power series approach. *Finance and Stochastics*, 13(2):269–303.
- Arribas, I. P., Salvi, C., and Szpruch, L. (2020). Sig-sdes model for quantitative finance. <https://arxiv.org/abs/2006.00218>.
- Bayer, C., Friz, P., and Gatheral, J. (2016). Pricing under rough volatility. *Quantitative Finance*, 16(6):887–904.
- Bayer, C., Hager, P. P., Riedel, S., and Schoenmakers, J. (2023). Optimal stopping with signatures. *Annals of Applied Probability*, 33(1):238–273.
- Benhamou, E., Gobet, E., and Miri, M. (2009). Smart expansion and fast calibration for jump diffusion. *Finance and Stochastics*, 13(4):563–589.
- Benhamou, E., Gobet, E., and Miri, M. (2010a). Expansion formulas for European options in a local volatility model. *International Journal of Theoretical and Applied Finance*, 13(4):603–634.
- Benhamou, E., Gobet, E., and Miri, M. (2010b). Time dependent Heston model. *SIAM Journal on Financial Mathematics*, 1:289–325.
- Bruned, Y., Hairer, M., and Zambotti, L. (2019). Algebraic renormalisation of regularity structures. *Inventiones mathematicae*, 215(3):1039–1156.
- Bühler, H., Horvath, B., Lyons, T., Arribas, I. P., and Wood, B. (2020). Generating financial markets with signatures. SSRN Electronic Journal. Available at SSRN: <https://ssrn.com/abstract=3657366>.

- Chen, K.-T. (1957). Integration of paths, geometric invariants and a generalized Baker–Hausdorff formula. *Annals of Mathematics*, 65(1):163–178.
- Chevyrev, I. and Kormilitzin, A. (2016). A primer on the signature method in machine learning. <https://arxiv.org/abs/1603.03788>.
- Comte, F. and Renault, E. (1998). Long memory in continuous-time stochastic volatility models. *Mathematical Finance*, 8(04):291–323.
- Cuchiero, C., Gazzani, G., Möller, J., and Svaluto-Ferro, S. (2025). Joint calibration to SPX and VIX options with signature-based models. *Mathematical Finance*, 35(1):161–213.
- Cuchiero, C., Gazzani, G., and Svaluto-Ferro, S. (2023). Signature-based models: Theory and calibration. *SIAM Journal on Financial Mathematics*, 14(3):910–957.
- De Santiago, R., Fouque, J. P., and Sølna, K. (2008). Bond markets with stochastic volatility. *Advances in Econometrics*, 22:215–242.
- Díaz, P. (2023). Rough volatility models using the signature transform: Theory and calibration. Master’s dissertation, Universitat de Barcelona. Supervisor: J. Vives.
- Fermanian, A. (2021). *Learning Time-Dependent Data with the Signature Transform*. Thèse de doctorat, Sorbonne Université. Discipline: Mathématiques appliquées, Spécialité: Statistique.
- Forde, M. and Jacquier, A. (2011). The large-maturity smile for the Heston model. *Finance and Stochastics*, 15(4):775–780.
- Forde, M., Jacquier, A., and Lee, R. (2011). The small-time smile and term structure of implied volatility under the Heston model. *SIAM Journal on Financial Mathematics*, 3(1):690–708.
- Forde, M., Jacquier, A., and Mijatović, A. (2010). Asymptotic formulae for implied volatility in the Heston model. *Proceedings of the Royal Society A*, 466(2124):3593–3620.
- Fouque, J. P., Papanicolaou, G., Sircar, K. R., and Sølna, K. (2003). Singular perturbations in option pricing. *SIAM Journal of Applied Mathematics*, 63(5):1648–1665.
- Friz, P. K. and Victoir, N. B. (2010). *Multidimensional Stochastic Processes as Rough Paths: Theory and Applications*, volume 120 of *Cambridge Studies in Advanced Mathematics*. Cambridge University Press, Cambridge.
- Fukasawa, M. (2017). Short-time at-the-money skew and rough fractional volatility. *Quantitative Finance*, 17(02):189–198.
- Gatheral, J., Jaisson, T., and Rosenbaum, M. (2018). Volatility is rough. *Quantitative Finance*, 18(6):933–949.
- Geng, X. (2021). An introduction to the theory of rough paths. Lecture notes, University of Melbourne, August 2021. Available at Xi Geng’s website.
- Hagan, P. S., Kumar, D., Lesniewski, A., and Woodward, D. E. (2002). Managing smile risk. *Willmot Magazine*, 15:84–108.
- Heston, S. L. (1993). A closed-form solution for options with stochastic volatility with applications to bond and currency options. *Review of Financial Studies*, 6(2):327–343.
- Hull, J. and White, A. (1987). The pricing of options on assets with stochastic volatilities. *Journal of Finance*, 42:281–300.
- Kalsi, J., Lyons, T., and Arribas, I. P. (2020). Optimal execution with rough path signatures. *SIAM Journal on Financial Mathematics*, 11(2):470–493.
- Lorig, M., Pagliarani, S., and Pascucci, A. (2013). Explicit implied volatilities for multifactor local-stochastic volatility models. *SSRN Electronic Journal*. Available at SSRN: <https://ssrn.com/abstract=2283874>.

- Lyons, T. and Qian, Z. (2002). *System control and rough paths*. Oxford University Press.
- Lyons, T. J. (1998). Differential equations driven by rough signals. *Revista Matemática Iberoamericana*, 14(2):215–310.
- Lyons, T. J., Caruana, M., and Lévy, T. (2007). *Differential Equations Driven by Rough Paths*, volume 1908 of *Lecture Notes in Mathematics*. Springer. Ecole d’Eté de Probabilités de Saint-Flour XXXIV-2004.
- Medvedev, A. and Scaillet, O. (2007). Approximation and calibration of short-term implied volatilities under jump-diffusion stochastic volatility. *Review of Financial Studies*, 20(02):427–459.
- Stein, E. M. and Stein, J. C. (1991). Stock price distributions with stochastic volatility: An analytic approach. *The Review of Financial Studies*, 4:727–752.
- Wiggins, J. (1987). Option values under stochastic volatilities. *Journal of Financial Economics*, 19:351–372.
- Young, L. C. (1936). An inequality of the Hölder type, connected with Stieltjes integration. *Acta Mathematica*, 67:251 – 282.